Supporting Information

Deep-blue phosphorescence from platinum(II) bis(acetylide) complexes with sulfur-bridged dipyridyl ligands

*Ka-Ming Tong, Jessica Toigo, Michael O. Wolf**

Department of Chemistry, University of British Columbia, Vancouver, British Columbia V6T 1Z1, Canada

Table of Contents **Page**

Experimental Section

Materials and Reagents. Solvents were reagent grade and used without any further purification. Potassium tetrachloroplatinate was purchased from Strem Chemicals. Phenylacetylene was purchased from Thermo Fisher Scientific Inc. Copper(I) iodide and poly(methyl methacrylate) (PMMA) were purchased from Sigma-Aldrich. Diisopropylamine was purchased from Alfa Aesar. The reference complex **[Pt(bpy)(C≡CPh)$_2$]**,[1] bis(pyridin-2-yl)sulfane (**DPS**), 2,2'-sulfinyldipyridine **(DPSO**), 2,2'-sulfonyldipyridine (**DPSO$_2$**), bis(4-methylpyridin-2-yl)sulfane (**MeDPS**), 2,2'-sulfinylbis(4-methylpyridine) (**MeDPSO**) and 2,2'-sulfonylbis(4-methylpyridine) (**MeDPSO$_2$**) were synthesized using literature methods.[2]

Synthesis. All experiments were performed under an inert atmosphere of nitrogen using standard Schlenk techniques unless otherwise stated.

***cis*-[Pt(DPS)Cl$_2$]**: To a solution of $K_2[PtCl_4]$ (50 mg, 0.120 mmol) in 15 mL of water was added **DPS** (mg, 0.120 mmol, 1.0 equiv), and acidified with 1.0 mL of 4 M HCl. The mixture was heated at 70 °C for 2 hours under nitrogen. The yellow precipitates were filtered off and washed with water, followed by ethanol and diethyl ether. The precipitates were then dried under reduced pressure to give pale yellow solids. Subsequent recrystallization from vapour diffusion of *n*-pentane into a dichloromethane solution of ***cis*-[Pt(DPS)Cl$_2$]** gave pale yellow crystals. Yield: 41 mg, 75%. ^{1}H NMR (CD_2Cl_2, 400 MHz): δ 9.19 (dd, *J* = 5.8, 1.3 Hz, 2H), 7.97–7.78 (m, 4H), 7.37 (ddd, *J* = 7.4, 5.9, 1.9 Hz, 2H). ^{13}C{^{1}H} NMR (CD_2Cl_2, 100 MHz): δ 156.01, 152.48, 139.84, 128.61, 125.90. HR-ESI MS *m/z* calcd $C_{10}H_8Cl_2N_2PtSNa$ $[M+Na]^+$: 475.9331; found, 475.9318.

***cis*-[Pt(DPSO)Cl$_2$]**: The complex was prepared according to a procedure similar to that for ***cis*-[Pt(DPS)Cl$_2$]**, except **DPSO** was used in place of **DPS**. Yield: 50 mg, 88%. ^{1}H NMR (CD_2Cl_2, 400 MHz): δ 9.12 (dd, *J* = 5.7, 0.8 Hz, 2H), 8.19 (td, *J* = 7.8, 1.5 Hz, 2H), 8.03 (m, 2H),

7.56 (ddd, *J* = 7.5, 5.7, 1.5 Hz, 2H). HR-ESI MS *m/z* calcd $C_{10}H_{12}Cl_2N_3OPtS$ $[M+NH_4]^+$: 486.9726; found, 486.9716.

***cis*-[Pt(DPSO$_2$)Cl$_2$]**: The complex was prepared according to a procedure similar to that for ***cis*-[Pt(DPS)Cl$_2$]**, except **DPSO$_2$** was used in place of **DPS**. Yield: 46 mg, 78%. ^{1}H NMR (CD_2Cl_2, 400 MHz): δ 9.48 (dd, *J* = 5.7, 0.8 Hz, 2H), 8.40 (dd, *J* = 7.8, 1.1 Hz, 2H), 8.27 (td, *J* = 7.8, 1.5 Hz, 2H), 7.74 (ddd, *J* = 7.5, 5.7, 1.6 Hz, 2H). HR-ESI MS *m/z* calcd $C_{10}H_8Cl_2N_2O_2PtSK$ $[M+K]^+$: 523.8968; found, 523.8959.

***cis*-[Pt(MeDPS)Cl$_2$]**: The complex was prepared according to a procedure similar to that for ***cis*-[Pt(DPS)Cl$_2$]**, except **MeDPS** was used in place of **DPS**. Subsequent recrystallization from vapour diffusion of *n*-pentane into a dichloromethane solution of ***cis*-[Pt(MeDPS)Cl$_2$]** gave pale yellow crystals. Yield: 36 mg, 62%. ^{1}H NMR (CD_2Cl_2, 400 MHz): δ 8.97 (d, *J* = 6.1 Hz, 2H), 7.65 (d, *J* = 2.0 Hz, 2H), 7.16 (dd, *J* = 6.1, 2.0 Hz, 2H), 2.39 (s, 6H). $^{13}C\{^1H\}$ NMR (CD_2Cl_2, 100 MHz): δ 154.85, 152.77, 151.67, 129.17, 126.67, 21.23. HR-ESI MS *m/z* calcd $C_{12}H_{16}Cl_2N_3PtS$ $[M+NH_4]^+$: 499.0090; found, 499.0077.

***cis*-[Pt(MeDPSO)Cl$_2$]**: The complex was prepared according to a procedure similar to that for ***cis*-[Pt(DPS)Cl$_2$]**, except **MeDPSO** was used in place of **DPS**. Yield: 54 mg, 90%. ^{1}H NMR (CD_2Cl_2, 400 MHz): δ 8.90 (d, *J* = 5.9 Hz, 2H), 7.81 (d, *J* = 2.0 Hz, 2H), 7.31 (dd, *J* = 5.5, 1.4 Hz, 2H), 2.50 (s, 6H). HR-ESI MS *m/z* calcd $C_{12}H_{16}Cl_2N_3OPtS$ $[M+NH_4]^+$: 515.0039; found, 515.0032.

***cis*-[Pt(MeDPSO$_2$)Cl$_2$]**: The complex was prepared according to a procedure similar to that for ***cis*-[Pt(DPS)Cl$_2$]**, except **MeDPSO$_2$** was used in place of **DPS**. Yield: 50 mg, 81%. ^{1}H NMR (CD_2Cl_2, 400 MHz): δ 9.26 (d, *J* = 5.9 Hz, 2H), 8.19 (d, *J* = 2.1 Hz, 2H), 7.51–7.49. (m, 2H), 2.50 (s, 6H). HR-ESI MS *m/z* calcd $C_{12}H_{16}Cl_2N_3O_2PtS$ $[M+NH_4]^+$: 530.9988; found, 530.9973.

***cis*-[Pt(DPS)(C≡CPh)$_2$] (1)**: To a suspension of ***cis*-[Pt(DPS)Cl$_2$]** (50 mg, 0.110 mmol) and CuI (2.10 mg, 0.0110 mmol, 0.1 equiv) in degassed dichloromethane–diisopropylamine was added phenylacetylene (45.0 µL, 0.440 mmol). The reaction mixture was stirred overnight at room temperature under an inert nitrogen atmosphere. After solvent removal under reduced pressure, the residue was dissolved in dichloromethane and then precipitated with *n*-hexane. The crude product was filtered and purified by column chromatography on silica gel using dichloromethane. Subsequent recrystallization from vapour diffusion of *n*-pentane into a dichloromethane solution of **1** gave pale yellow crystals. Yield: 47 mg, 73%. ^{1}H NMR ($CDCl_3$, 400 MHz): δ 9.49 (dd, *J* = 5.6, 1.7 Hz, 2H), 7.86 (td, *J* = 7.7, 1.8 Hz, 2H), 7.81–7.79 (m, 2H), 7.42–7.38 (m, 4H), 7.35 (ddd, *J* = 7.3, 5.7, 1.6 Hz, 2H), 7.23–7.14 (m, 4H), 7.11–7.06 (m, 2H). ^{13}C{^{1}H} NMR (CD_2Cl_2, 100 MHz): δ 155.32, 151.70, 139.23, 131.73, 128.76, 127.88, 127.78, 125.49, 100.35, 82.14. IR (solid) ν/ cm^{-1}: 2112, 2128(sh) ν(C≡C). HR-ESI MS *m/z* calcd $C_{26}H_{19}N_2PtS$ $[M+H]^+$: 586.0917; found, 586.0914.

***cis*-[Pt(DPSO)(C≡CPh)$_2$] (2)**: The complex was prepared according to a procedure similar to that for **1**, except ***cis*-[Pt(DPSO)Cl$_2$]** was used in place of ***cis*-[Pt(DPS)Cl$_2$]**. Subsequent recrystallization from vapour diffusion of *n*-pentane into a dichloromethane solution of **2** gave pale yellow crystals. Yield: 41 mg, 64%. ^{1}H NMR (CD_2Cl_2, 400 MHz): δ 9.30 (dd, *J* = 5.5, 0.9 Hz, 2H), 8.18 (td, *J* = 7.8, 1.6 Hz, 2H), 8.12–8.07 (m, 2H), 7.56 (ddd, *J* = 7.2, 5.4, 1.5 Hz, 2H), 7.37–7.29 (m, 4H), 7.25–7.17 (m, 4H), 7.16–7.09 (m, 2H). ^{13}C{^{1}H} NMR (CD_2Cl_2, 100 MHz): δ 160.96, 154.49, 140.69, 132.16, 128.23, 127.83, 127.71, 126.24, 122.21, 101.63, 81.24. IR (solid) ν/ cm^{-1}: 2117, 2131 ν(C≡C). HR-ESI MS *m/z* calcd $C_{26}H_{19}N_2OPtS$ $[M+H]^+$: 602.0866; found, 602.0860.

***cis*-[Pt(DPSO$_2$)(C≡CPh)$_2$] (3)**: The complex was prepared according to a procedure similar to that for **1**, except ***cis*-[Pt(DPSO$_2$)Cl$_2$]** was used in place of ***cis*-[Pt(DPS)Cl$_2$]**. Yield: 21 mg, 33%. ^{1}H NMR (CD_2Cl_2, 400 MHz): δ 9.73 (dd, *J* = 5.7, 1.2 Hz, 2H), 8.45 (dd, *J* = 7.9, 0.8 Hz, 2H), 8.28 (td, *J* = 7.9, 1.6 Hz, 2H), 7.77 (ddd, *J* = 7.8, 5.5, 1.5 Hz, 2H), 7.39 (dd, *J* = 8.2, 1.3 Hz, 4H), 7.29–7.21 (m, 4H), 7.19–7.12 (m, 2H). ^{13}C{^{1}H} NMR (CD_2Cl_2, 100 MHz): δ 156.47, 152.27,

140.79, 132.30, 130.92, 128.26, 127.85, 126.29, 125.99, 101.10, 78.75. IR (solid) ν/ cm^{-1}: 2120, 2133(sh) ν(C≡C). HR-ESI MS *m/z* calcd $C_{26}H_{19}N_2O_2PtS$ $[M+H]^+$: 618.0815; found, 618.0804.

***cis*-[Pt(MeDPS)(C≡CPh)$_2$] (4)**: The complex was prepared according to a procedure similar to that for **1**, except ***cis*-[Pt(MeDPS)Cl$_2$]** was used in place of ***cis*-[Pt(DPS)Cl$_2$]**. Yield: 39 mg, 61%. ^{1}H NMR (CD_2Cl_2, 400 MHz): δ 9.23 (dd, *J* = 5.8Hz, 2H), 7.73–7.64 (m, 2H), 7.42–7.30 (m, 4H), 7.27–7.17 (m, 6H), 7.15–7.07 (m, 2H), 2.38 (s, 6H). $^{13}C\{^1H\}$ NMR (CD_2Cl_2, 100 MHz): δ 154.79, 152.33, 151.46, 132.11, 129.65, 128.43, 128.16, 126.68, 125.77, 100.46, 83.25. IR (solid) ν/ cm^{-1}: 2113, 2125 ν(C≡C). HR-ESI MS *m/z* calcd $C_{28}H_{23}N_2OPtS$ $[M+H]^+$: 614.1230; found, 614.1226.

***cis*-[Pt(MeDPSO)(C≡CPh)$_2$] (5)**: The complex was prepared according to a procedure similar to that for **1**, except ***cis*-[Pt(MeDPSO)Cl$_2$]** was used in place of ***cis*-[Pt(DPS)Cl$_2$]**. Subsequent recrystallization from vapour diffusion of *n*-pentane into a 1,2-dichloroethane solution of **5** gave pale yellow crystals. Yield: 39 mg, 62%. ^{1}H NMR (CD_2Cl_2, 400 MHz): δ 9.12 (d, *J* = 5.6 Hz, 2H), 7.91 (s, 2H), 7.39–7.32 (m, 6H), 7.26–7.19 (m, 4H), 7.17–7.10 (m, 2H), 2.49 (s, 6H). $^{13}C\{^1H\}$ NMR (CD_2Cl_2, 100 MHz): δ 160.20, 153.91, 153.68, 132.13, 128.53, 128.19, 127.85, 126.11, 122.55, 101.33, 81.85, 21.99. IR (solid) ν/ cm^{-1}: 2109, 2128 ν(C≡C). HR-ESI MS *m/z* calcd $C_{28}H_{22}N_2OPtSNa$ $[M+Na]^+$: 652.0998; found, 652.0993.

***cis*-[Pt(MeDPSO$_2$)(C≡CPh)$_2$] (6)**: The complex was prepared according to a procedure similar to that for **1**, except ***cis*-[Pt(MeDPSO$_2$)Cl$_2$]** was used in place of ***cis*-[Pt(DPS)Cl$_2$]**. Subsequent recrystallization from vapour diffusion of *n*-pentane into a 1,2-dichloroethane solution of **6** gave pale yellow crystals. Yield: 28 mg, 45%. ^{1}H NMR (CD_2Cl_2, 400 MHz): δ 9.51 (d, *J* = 5.5 Hz, 2H), 8.24 (d, *J* = 1.9 Hz, 2H), 7.54 (dd, *J* = 5.7, 1.1 Hz, 2H), 7.38 (m, 4H), 7.23 (t, *J* = 7.5 Hz, 4H), 7.15 (m, 2H), 2.50 (s, 6H). $^{13}C\{^1H\}$ NMR (CD_2Cl_2, 100 MHz): δ 155.56, 154.07, 151.52,

132.21, 131.32, 128.19, 127.94, 126.49, 126.11, 100.66, 79.51, 21.96. IR (solid) ν/ cm^{-1}: 2121, 2135 ν(C≡C). HR-ESI MS *m/z* calcd $C_{28}H_{23}N_2O_2PtS$ $[M+H]^+$: 646.1119; found, 646.1128.

PMMA Film Fabrication. A solution of PMMA (98 mg) and the respective platinum complex (2 mg, 2 wt%) in dichloromethane (1 mL) was prepared. The solution was drop-coated onto a quartz plate and then dried overnight at room temperature prior to use.

Physical Measurements and Instrumentation. ^{1}H NMR spectra were collected using a Bruker AV-400 (400 MHz) spectrometer at room temperature and referenced to the residual protonated solvent peak. NMR solvent from Cambridge Isotope Laboratories was used as received. Infrared spectroscopy was performed on an attenuated total reflection (ATR) crystal using a PerkinElmer Frontier FT-IR spectrometer. High-resolution electrospray ionization (HR-ESI) mass spectrometry data were obtained on a Waters/Micromass LCT TOF-MS spectrometer. HPLC grade solvents were used for spectroscopic analysis. Thermogravimetric analysis (TGA) was performed on a Netzsch TGA209 F1 Libra thermogravimetric analyzer under N_2, samples were heated from 30 to 600 °C at the rate of 10 °C/min. Electronic absorption spectra were obtained on a Varian-Cary 5000 UV-vis-near-IR spectrophotometer. Photoluminescence spectra at room temperature were collected using an Edinburgh Instrument FLS100 spectrofluorometer. Solution samples were maintained under a blanket of Ar for the duration of the measurements in 1 cm^2 quartz cells (Starna Cells) fitted with a rubber septum. Measurements of the 2-MeTHF glass samples at 77 K were carried with the solutions in a quartz tube inside a liquid nitrogen filled quartz optical Dewar flask fitted to an Edinburgh Instrument FLS1000 spectrofluorometer. Emission lifetime data were obtained using a Horiba Yvon Fluorocube TCSPC apparatus using a 375 nm laser excitation source with a 400 nm long-pass filter between sample and detector. Lifetime data were fitted against the laser source background using the DAS6 Data Analysis software package. The photoluminescence quantum yields of the solution state samples were measured using the

method by Demas and Crosby using quinine sulfate in 0.1 M aqueous sulfuric acid (Φ_{em} = 0.54) as a reference standard.[3] Photoluminescence quantum yields of the solid-state samples were determined using an Edinburgh Instruments barium sulfate coated integrating sphere fitted in a FS5 spectrofluorometer. Cyclic voltammetric measurements were performed on a CHI 660D potentiostat with a 3-electrode configuration using a platinum working electrode, silver wire pseudo-reference electrode and platinum mesh counter electrode. The electrochemical measurements were performed in acetonitrile solution with 0.1 M $^{n}Bu_4NPF_6$ as electrolyte and 0.1 mM of each complex. The solution was degassed with Ar and a scan rate of 100 mVs^{-1} was used in all cases. Potentials were referenced to Fc/Fc^{+} with the addition of ferrocene at the end of each experiment.

X-ray Crystallography. Single crystal diffraction data were collected using a Bruker APEX DUO diffractometer with graphite monochromated Mo Kα radiation (λ = 0.71073 Å) at 100 K. Raw frame data were processed using APEX3. The program SAINT[4] was used to reduce the data and the program SADABS[5] was used to make corrections to the empirical absorptions. Space group assignments were made using XPREP on all compounds. The structures were solved in the Olex2 [6] suite of programs using Intrinsic Phasing and refined using full-matrix least-squares/difference Fourier techniques on F2 using SHELXL.[7] All non-hydrogen atoms were refined anisotropically. Diagrams and publications materials were generated using ORTEP-3, Mercury and PLATON.

Theoretical methods. Geometry optimizations for complexes **1**–**6** were carried out using density functional theory (DFT) in vacuum with the Orca 5.0.2 software package[8] and the images of the complexes were obtained using the GaussView 6 program. The PBE0 functional[9] with basis set SARC-ZORA-TZVP for Pt(II) atom, and the Def2-TZVP(-f) for the other atoms was employed to optimize the geometry of the ground states (S_0) and lowest-energy triplet states (T_1), using the scalar-relativistic method ZORA to account for relativistic effects.[10] Grimme's dispersion

correction with damping D3BJ and the resolution of identity approximation for the Coulomb part, with the corresponding auxiliary basis, were also included.[11] Analytical harmonic vibrational frequency calculations were performed to confirm that the ground state represents the lowest energy point on the potential energy surface. Time-dependent density functional theory (TD-DFT)[12] was employed to obtain the first 50 singlet excited states while also incorporating a solvent correction with a continuous polarizability model method (CPCM).[13] Quasi-degenerate perturbation theory was utilized to conduct the SOC calculations in addition to the TD-DFT results.[14]

NMR Spectra

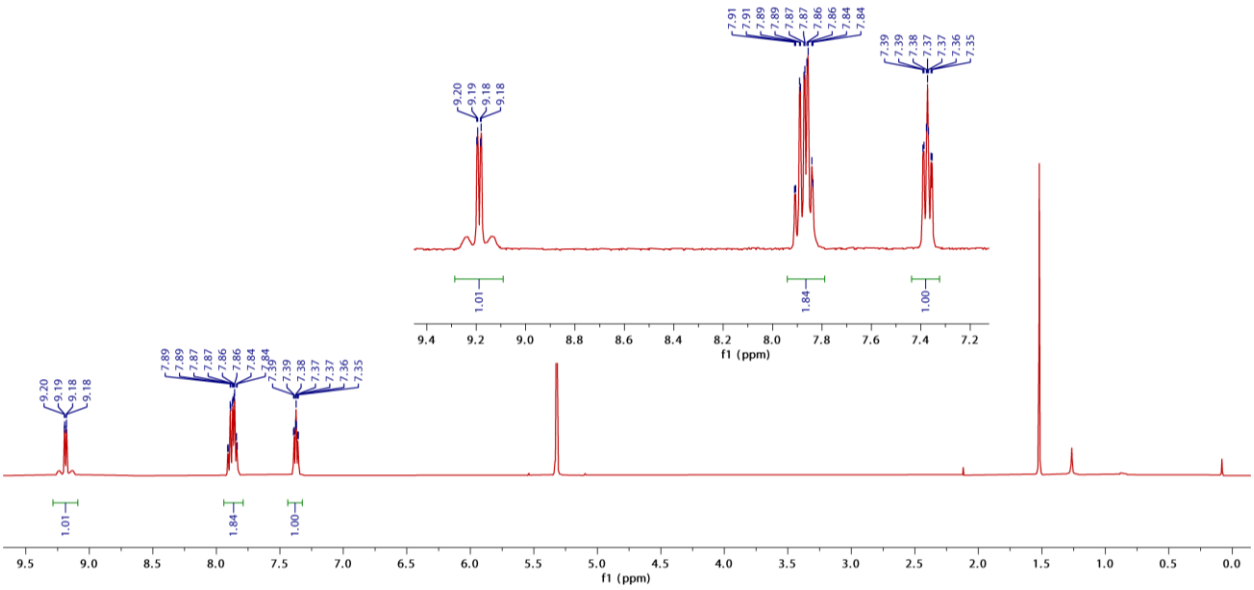

Figure S1. ^{1}H NMR spectrum of **[Pt(DPS)Cl$_2$]** in CD_2Cl_2.

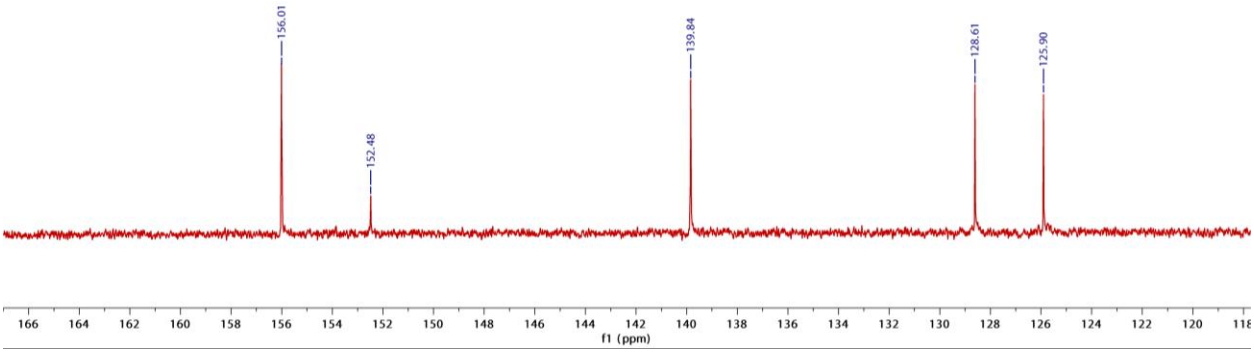

Figure S2. $^{13}C\{^{1}H\}$ NMR spectrum of **[Pt(DPS)Cl$_2$]** in CD_2Cl_2.

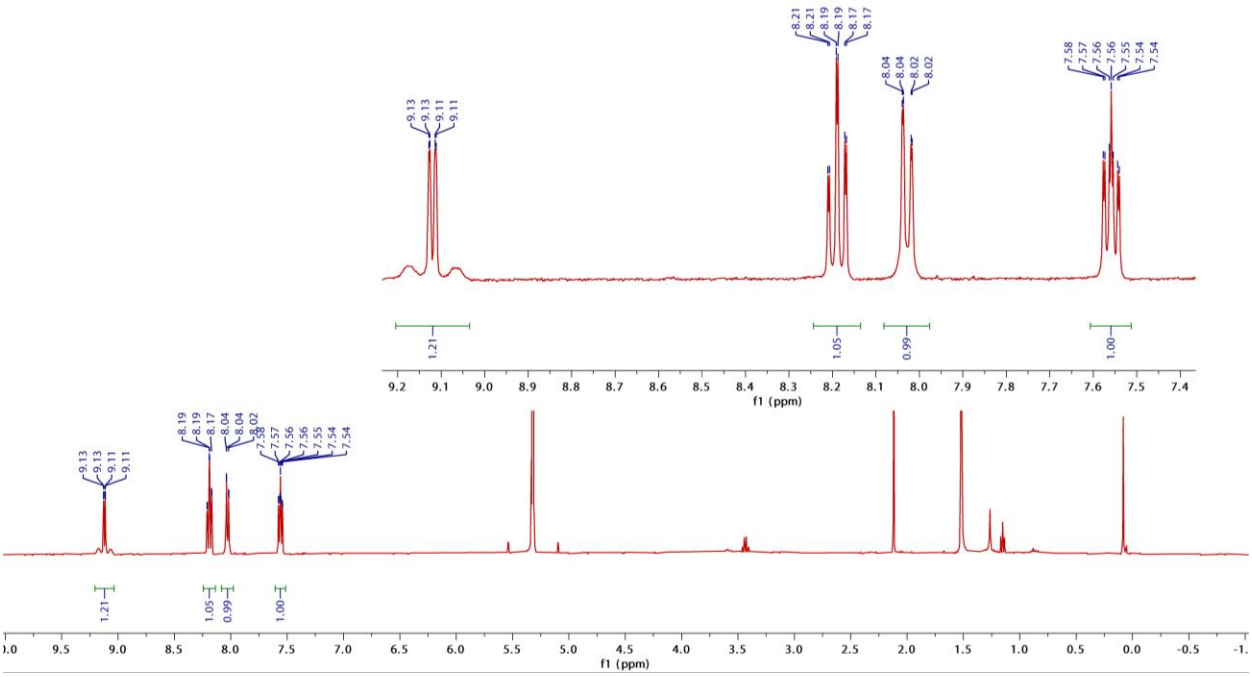

Figure S3. ^{1}H NMR spectrum of **[Pt(DPSO)Cl$_2$]** in CD_2Cl_2.

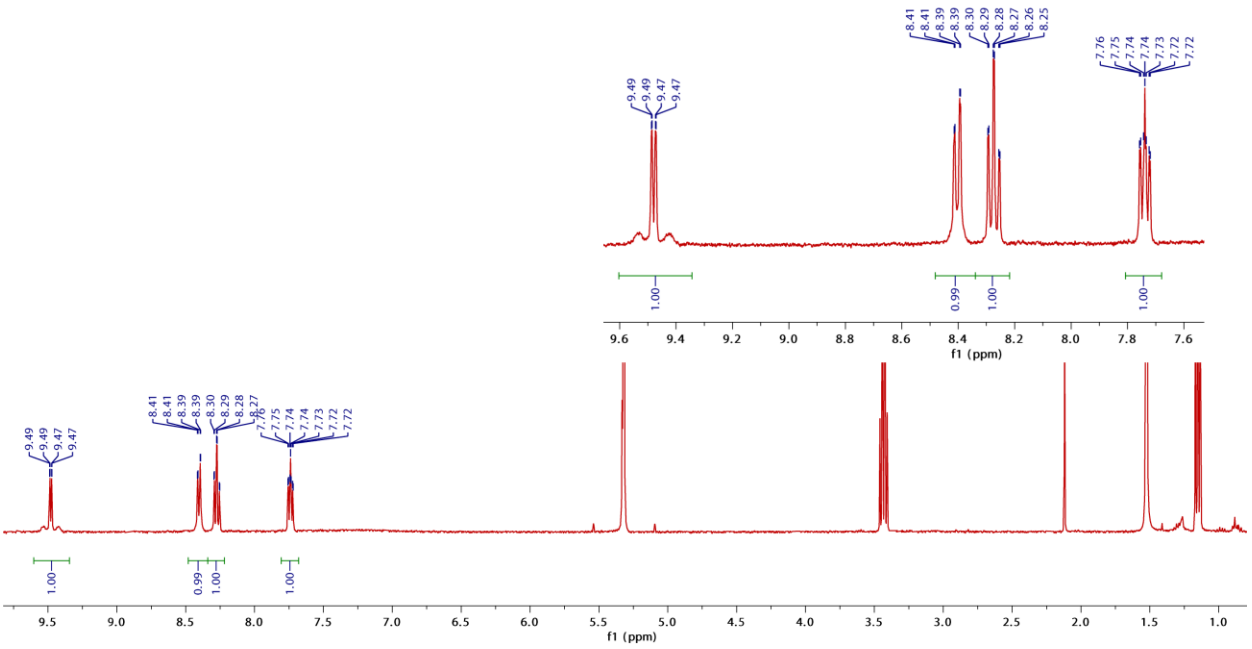

Figure S4. ^{1}H NMR spectrum of **[Pt(DPSO$_2$)Cl$_2$]** in CD_2Cl_2.

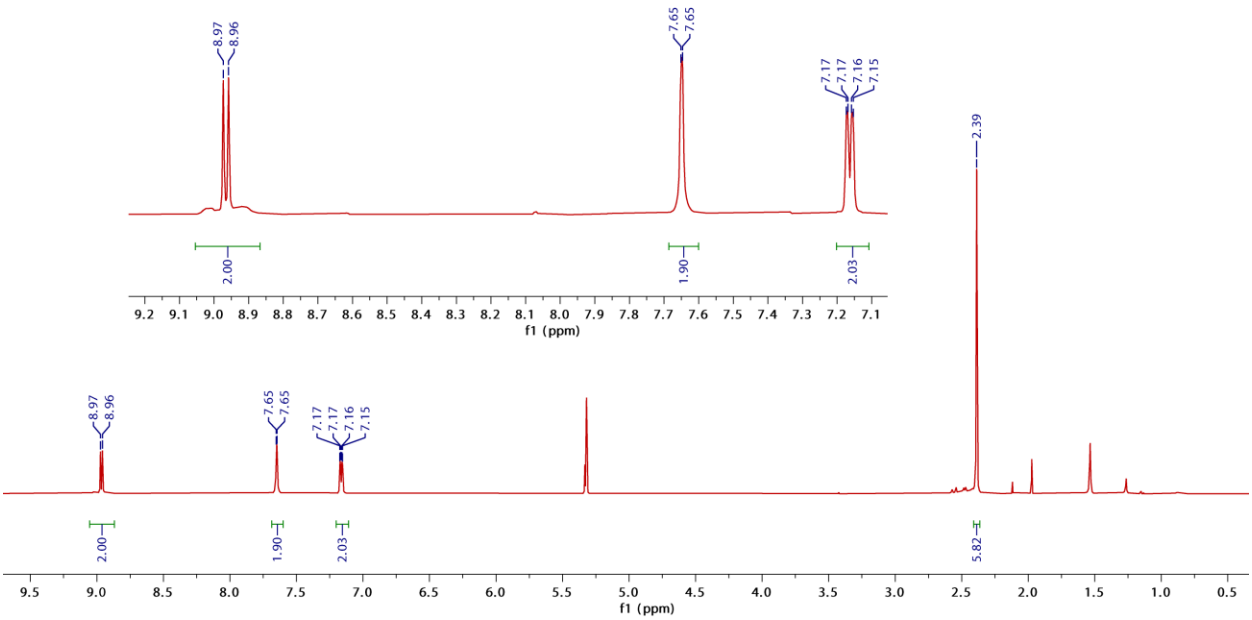

Figure S5. ^{1}H NMR spectrum of **[Pt(MeDPS)Cl$_2$]** in CD_2Cl_2.

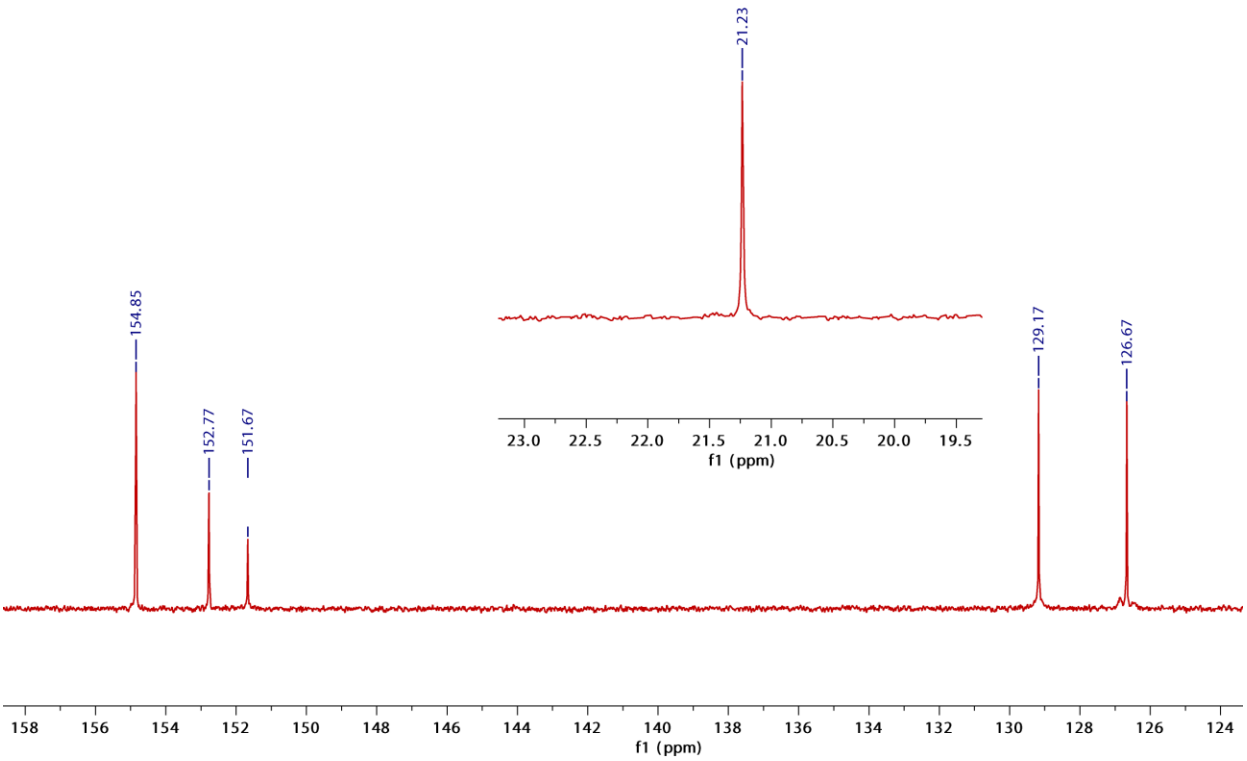

Figure S6. ^{13}C{^{1}H} NMR spectrum of **[Pt(MeDPS)Cl$_2$]** in CD_2Cl_2.

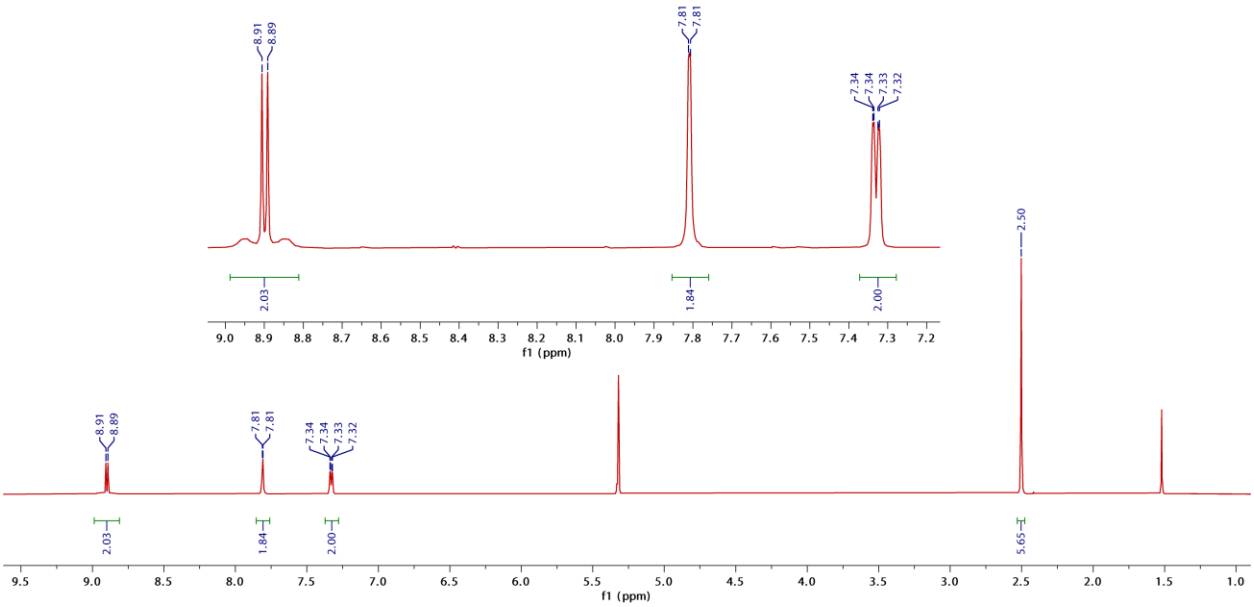

Figure S7. ^{1}H NMR spectrum of **[Pt(MeDPSO)Cl$_2$]** in CD_2Cl_2.

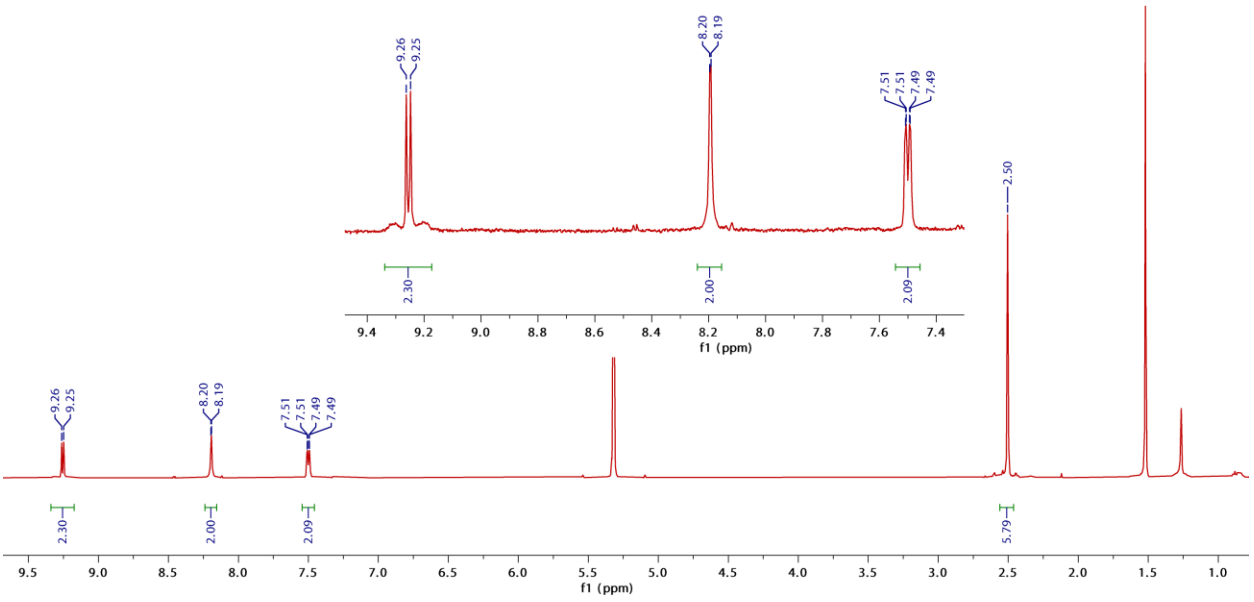

Figure S8. ^{1}H NMR spectrum of **[Pt(MeDPSO$_2$)Cl$_2$]** in CD_2Cl_2.

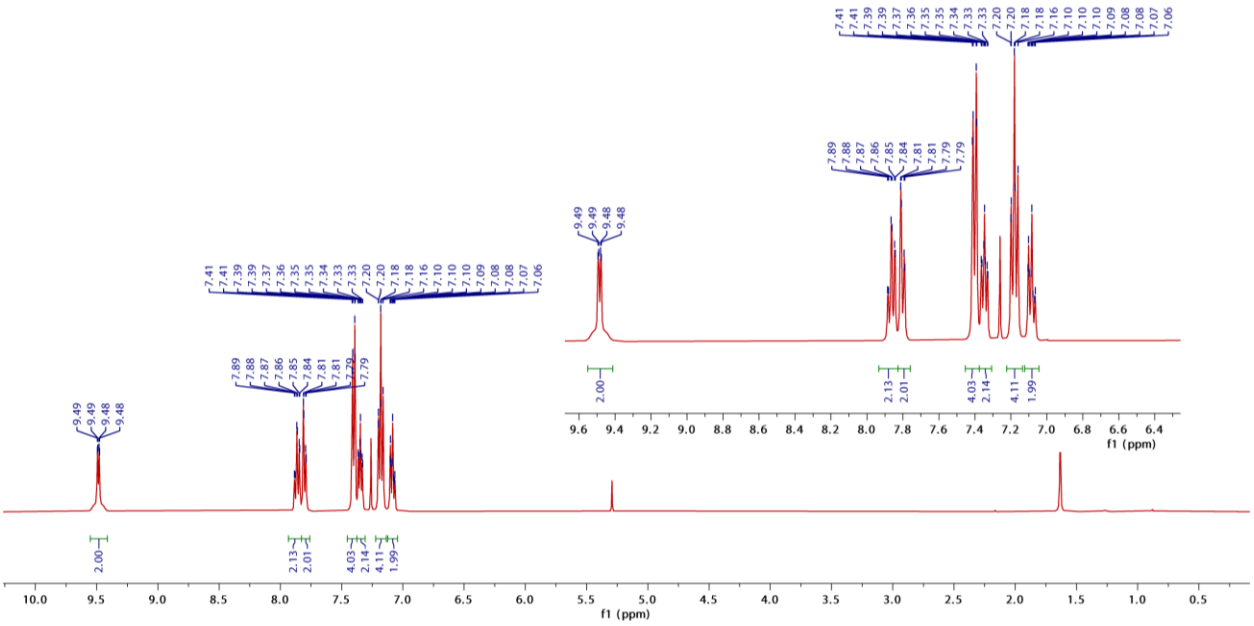

Figure S9. ^{1}H NMR spectrum of **1** in $CDCl_3$.

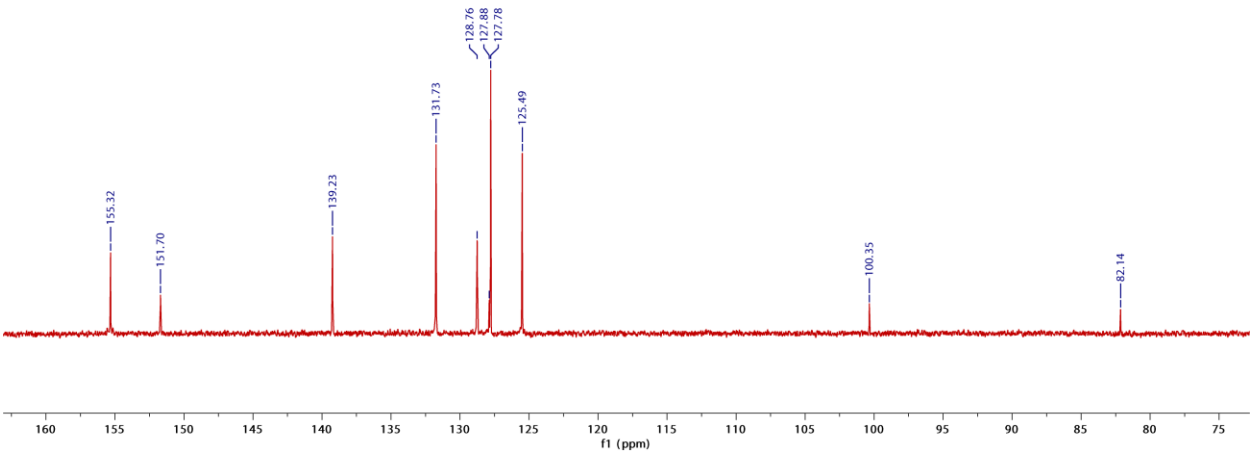

Figure S10. $^{13}C\{^{1}H\}$ NMR spectrum of **1** in CD_2Cl_2.

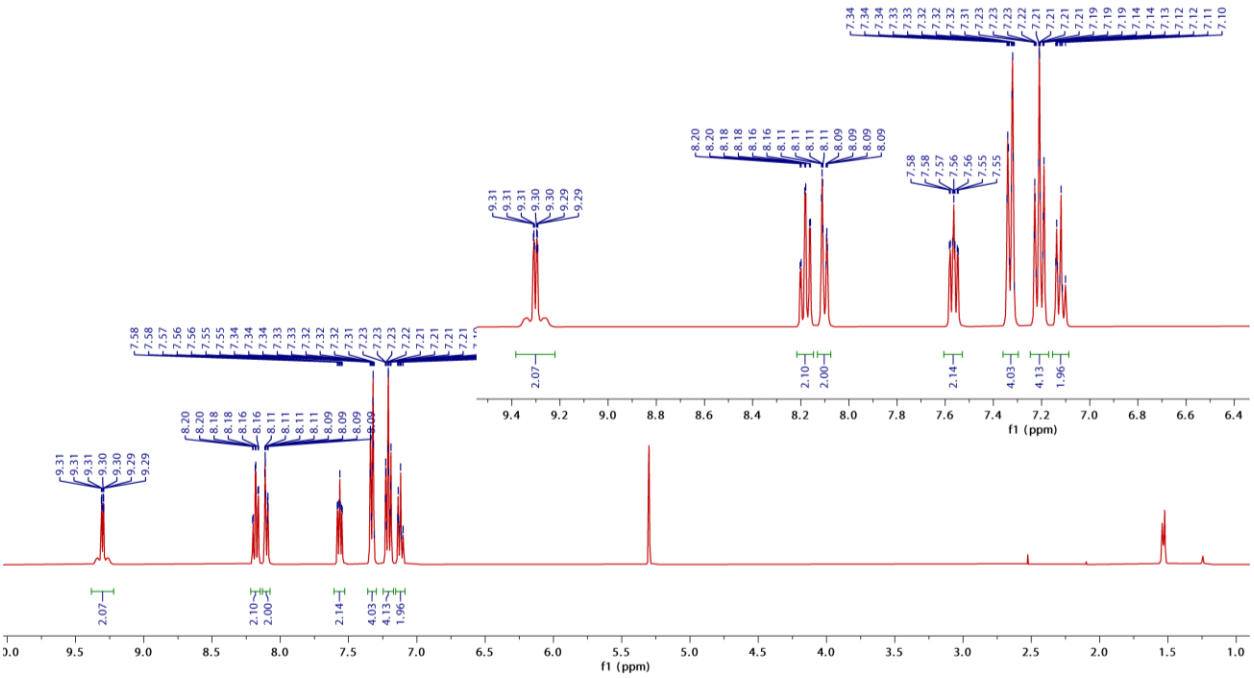

Figure S11. ^{1}H NMR spectrum of **2** in CD_2Cl_2.

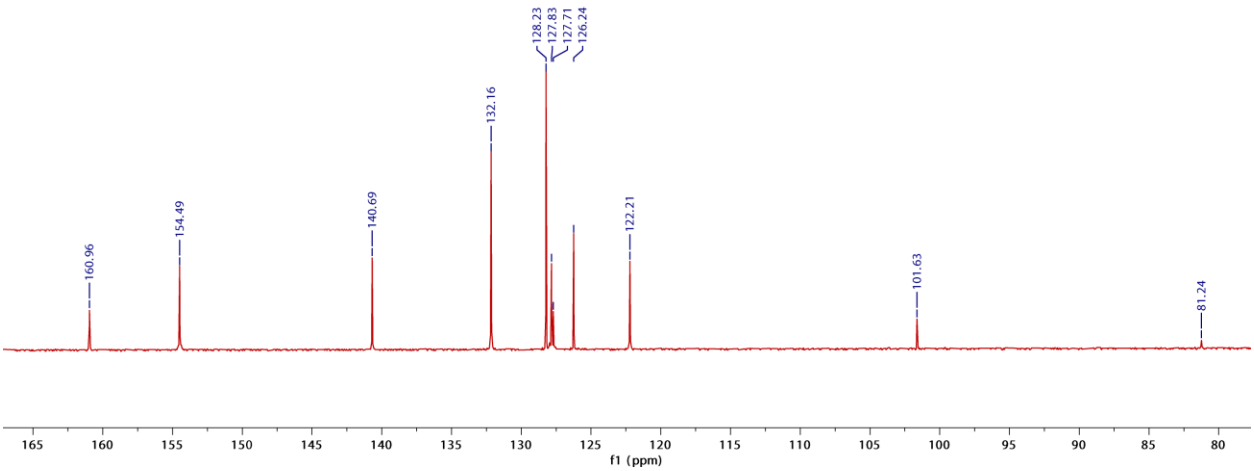

Figure S12. $^{13}C\{^{1}H\}$ NMR spectrum of **2** in CD_2Cl_2.

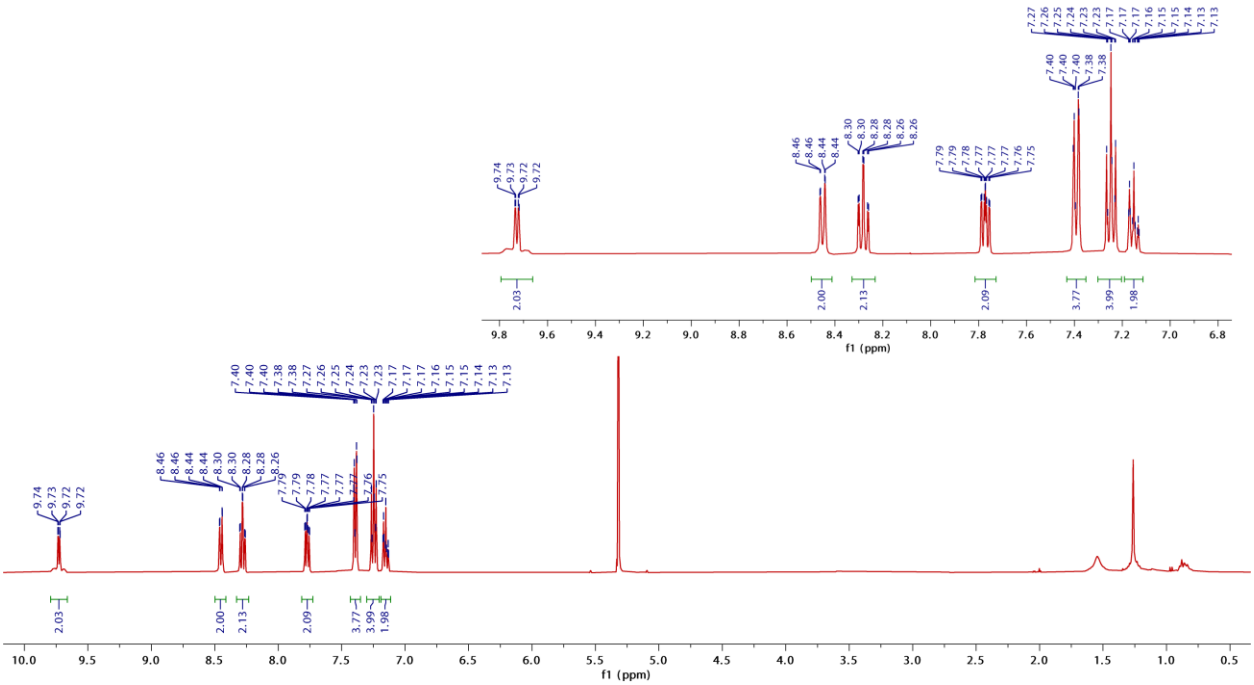

Figure S13. ^{1}H NMR spectrum of **3** in CD_2Cl_2.

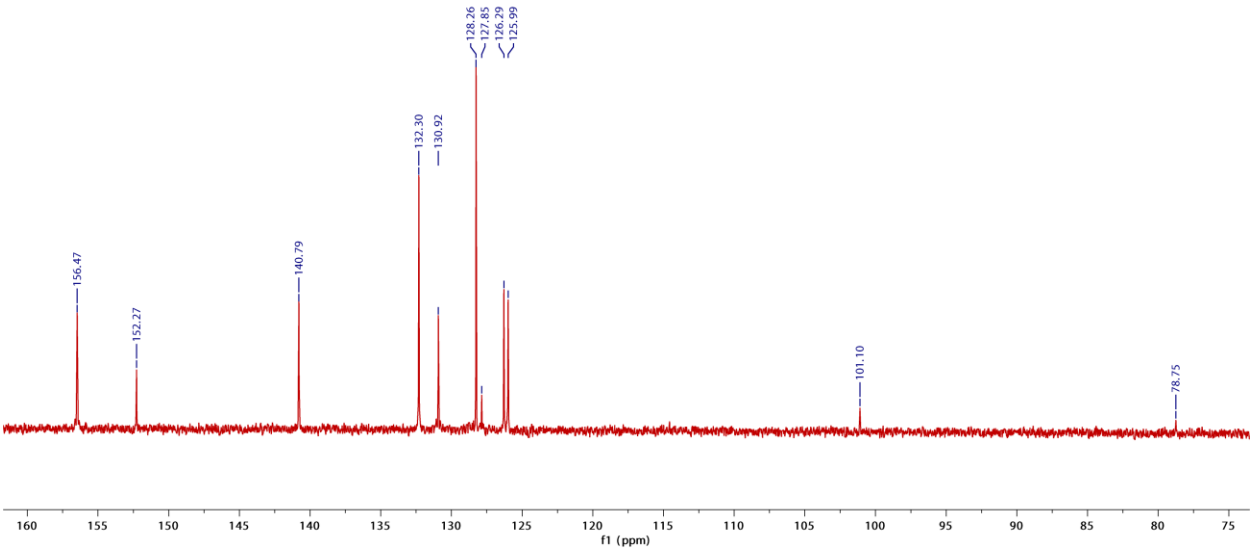

Figure S14. $^{13}C\{^{1}H\}$ NMR spectrum of **3** in CD_2Cl_2.

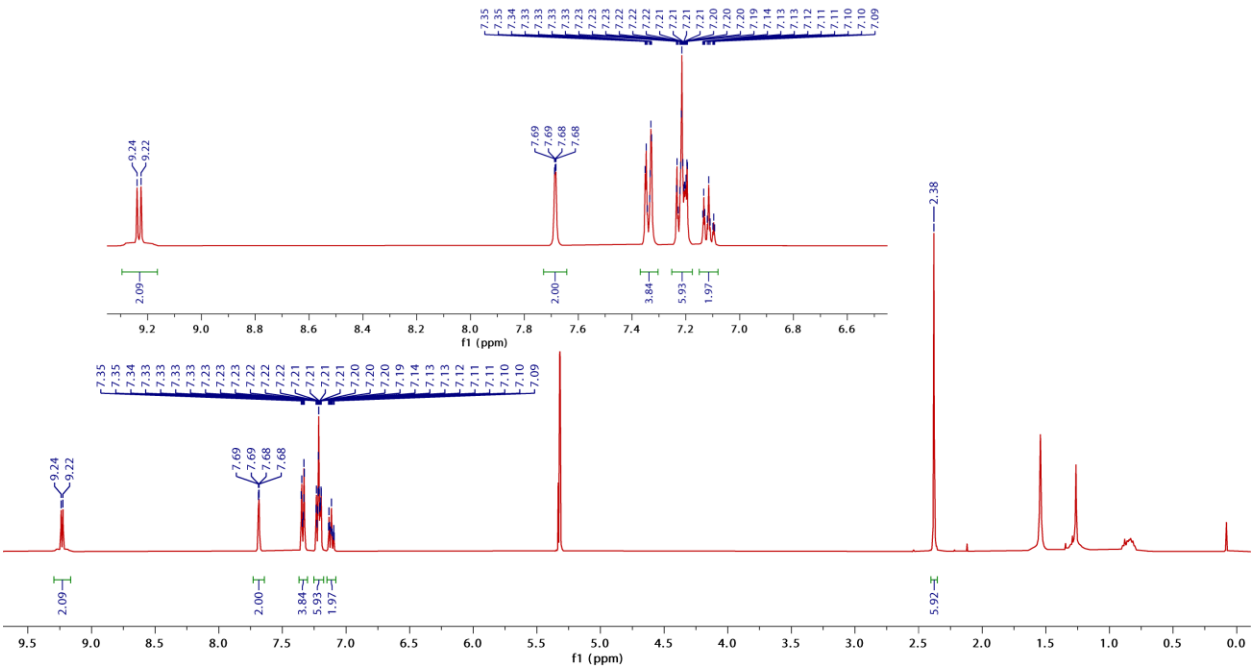

Figure S15. ^{1}H NMR spectrum of **4** in CD_2Cl_2.

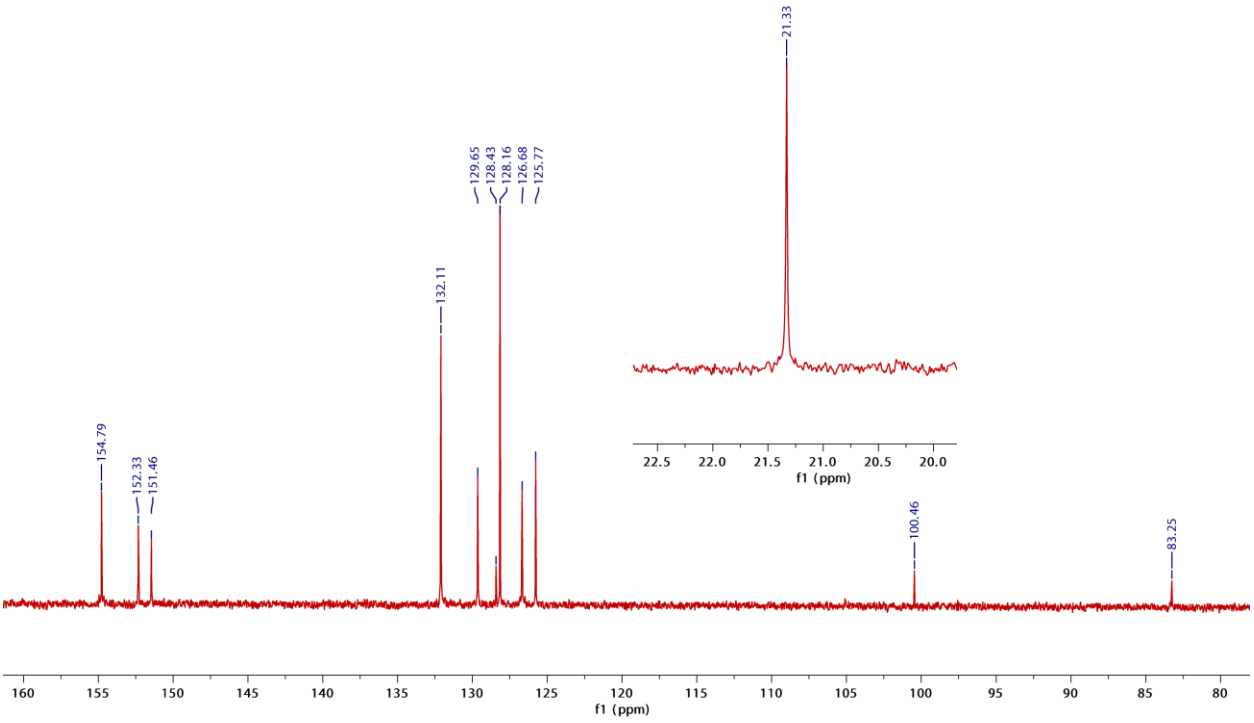

Figure S16. $^{13}C\{^{1}H\}$ NMR spectrum of **4** in CD_2Cl_2.

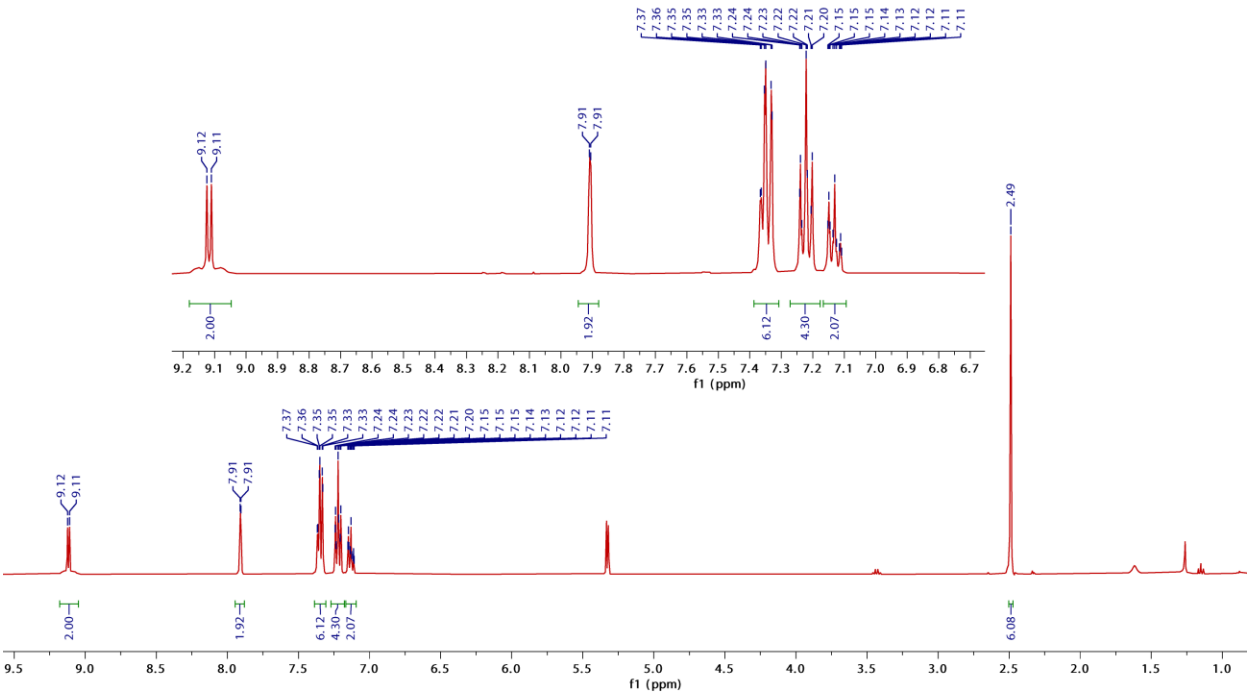

Figure S17. ^{1}H NMR spectrum of **5** in CD_2Cl_2.

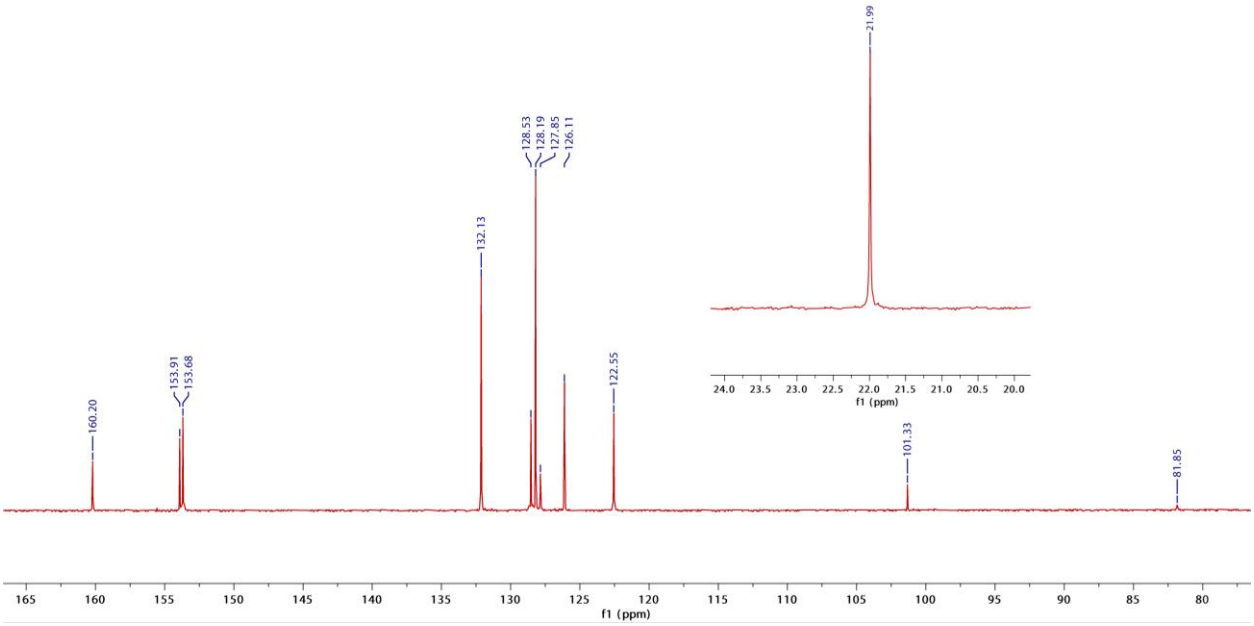

Figure S18. $^{13}C\{^{1}H\}$ NMR spectrum of **5** in CD_2Cl_2.

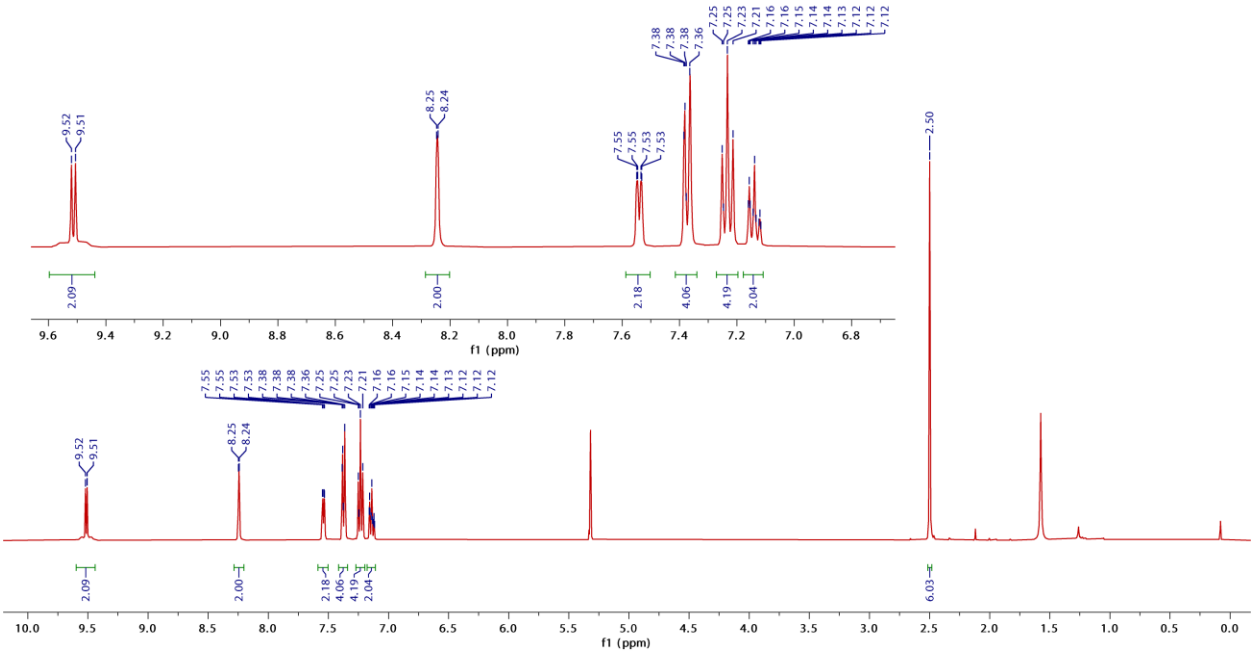

Figure S19. ^{1}H NMR spectrum of **6** in CD_2Cl_2.

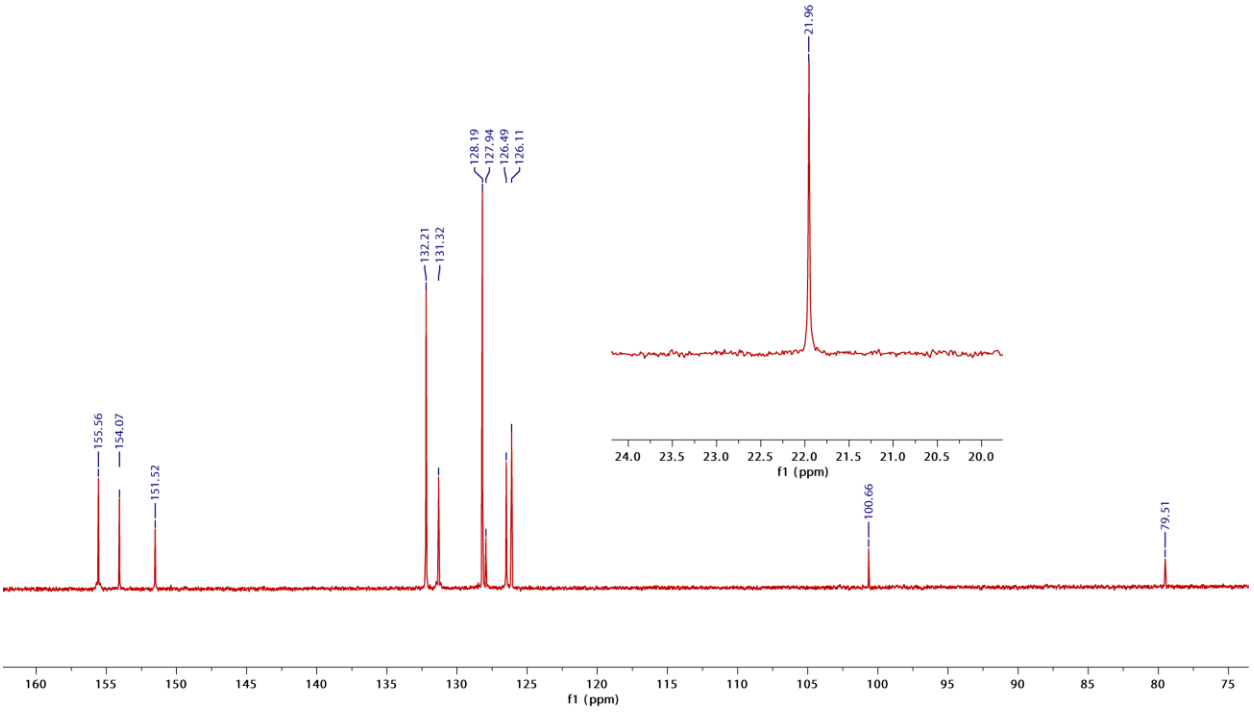

Figure S20. ^{13}C{^{1}H} NMR spectrum of **6** in CD_2Cl_2.

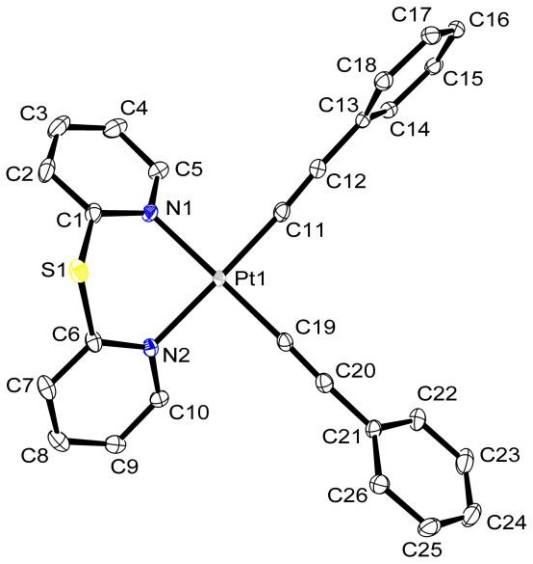

Figure S21. Crystal structure of complex **1**. Ellipsoids are plotted at the 50% probability level, and H atoms are removed for clarity.

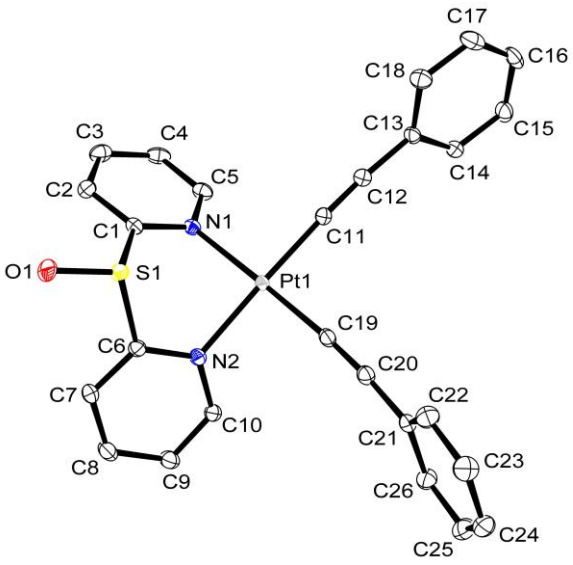

Figure S22. Crystal structure of complex **2**. Ellipsoids are plotted at the 50% probability level, and H atoms are removed for clarity.

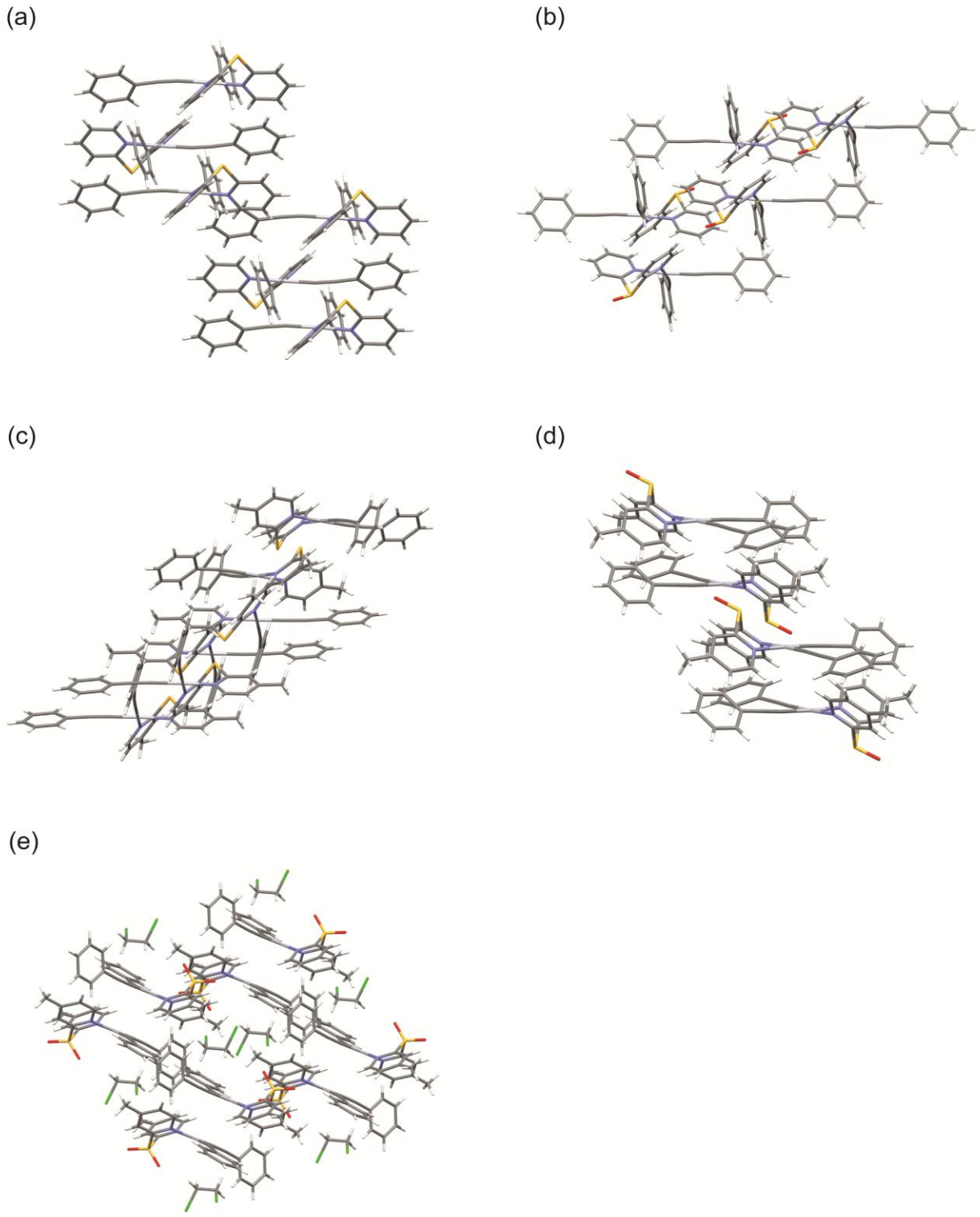

Figure S23. Molecular packing of the complexes (a) **1**, (b) **2**, (c) **4**, (d) **5** and (e) **6**.

Table S1. Crystal and structure determination data for **1**.

Formula	$C_{26}H_{18}N_2PtS$
Molecular weight	585.57
T / K	100
a / Å	11.2341(5)
b / Å	13.2688(6)
c / Å	17.1255(8)
α / deg	67.6220(10)
β / deg	89.7200(10)
γ / deg	65.4480(10)
V/ Å^3	2111.14(17)
Crystal color	yellow
Crystal system	triclinic
Space group	P$\bar{1}$
Z	4
F(000)	1128
D_c / gcm^{-3}	1.842
Crystal dimensions / mm	0.37 × 0.29 × 0.21
λ / Å	0.71073
μ / mm^{-1}	6.761
Collection range	$1.308 \leq \theta \leq 30.664°$ (h: −16 to 16; k: −19 to 15; l: −24 to 24)
Completeness to theta	0.996
No. of data collected	84801
No. of unique data	13013
No. of data used in refinement, m	11810
No. of parameters refined, p	541
R	0.0139
wR	0.0304
Goodness-of-fit, S	1.041
Maximum shift, $(\Delta/\sigma)_{max}$	0.007
Residual extrema in final difference map, eÅ^{-3}	+0.857, −0.842

Table S2. Crystal and structure determination data for complex **2**.

Formula	$C_{26}H_{18}N_2OPtS$
Molecular weight	601.57
T / K	100
a / Å	7.9676(5)
b / Å	11.9940(7)
c / Å	12.5963(7)
α / deg	117.4240(10)
β / deg	97.964(2)
γ / deg	90.392(2)
V/ Å^3	1054.74(11)
Crystal color	yellow
Crystal system	triclinic
Space group	P$\bar{1}$
Z	2
F(000)	580
D_c / gcm^{-3}	1.894
Crystal dimensions / mm	0.12 × 0.06 × 0.02
λ / Å	0.71073
μ / mm^{-1}	6.772
Collection range	1.845 ≤ θ ≤ 33.319° (*h*: −12 to 12; *k*: −18 to 16; *l*: 0 to 19)
Completeness to theta	0.922
No. of data collected	7534
No. of unique data	7534
No. of data used in refinement, *m*	6912
No. of parameters refined, *p*	280
R	0.0191
wR	0.0396
Goodness-of-fit, S	1.076
Maximum shift, $(\Delta/\sigma)_{max}$	0.004
Residual extrema in final difference map, eÅ^{-3}	+1.238, −0.790

Table S3. Crystal and structure determination data for complex **4**.

Formula	$C_{28}H_{22}N_2PtS$
Molecular weight	613.62
T / K	100
a / Å	10.8444(10)
b / Å	11.2925(10)
c / Å	18.7020(17)
α / deg	90
β / deg	96.706(2)
γ / deg	90
V/ Å^3	2274.6(4)
Crystal color	yellow
Crystal system	monoclinic
Space group	$P2_1/n$
Z	4
F(000)	1192
D_c / gcm^{-3}	1.792
Crystal dimensions / mm	0.20 × 0.20 × 0.19
λ / Å	0.71073
μ / mm^{-1}	6.279
Collection range	$2.072 \leq \theta \leq 30.563°$ (h: −15 to 15; k: −16 to 16; l: −26 to 26)
Completeness to theta	0.999
No. of data collected	82611
No. of unique data	6980
No. of data used in refinement, m	6556
No. of parameters refined, p	291
R	0.0133
wR	0.0286
Goodness-of-fit, S	1.104
Maximum shift, $(\Delta/\sigma)_{max}$	0.009
Residual extrema in final difference map, eÅ^{-3}	+0.996, −0.775

Table S4. Crystal and structure determination data for complex **5**.

Formula	$C_{28}H_{22}N_2OPtS$
Molecular weight	629.62
T / K	100
a / Å	9.2869(7)
b / Å	12.7332(9)
c / Å	21.2615(15)
α / deg	89.275(2)
β / deg	82.262(2)
γ / deg	71.515(2)
V/ Å^3	2361.6(3)
Crystal color	yellow
Crystal system	triclinic
Space group	P$\bar{1}$
Z	4
F(000)	1224
D_c / gcm^{-3}	1.771
Crystal dimensions / mm	0.36 × 0.35 × 0.03
λ / Å	0.71073
μ / mm^{-1}	6.053
Collection range	$0.967 \leq \theta \leq 30.667°$ (*h*: −13 to 13; *k*: −18 to 18; *l*: −30 to 30)
Completeness to theta	0.993
No. of data collected	72022
No. of unique data	14535
No. of data used in refinement, *m*	12825
No. of parameters refined, *p*	599
R	0.0210
wR	0.0454
Goodness-of-fit, S	1.036
Maximum shift, $(\Delta/\sigma)_{max}$	0.005
Residual extrema in final difference map, eÅ^{-3}	+2.423, −0.962

Table S5. Crystal and structure determination data for complex **6**.

Formula	$C_{28}H_{22}N_2O_2PtS \bullet C_2H_4Cl_2$
Molecular weight	744.58
T / K	100
a / Å	10.5828(8)
b / Å	26.522(2)
c / Å	9.9870(8)
α / deg	90
β / deg	99.343(2)
γ / deg	90
V/ Å^3	2765.9(4)
Crystal color	yellow
Crystal system	monoclinic
Space group	$P2_1/c$
Z	4
F(000)	1456
D_c / gcm^{-3}	1.788
Crystal dimensions / mm	0.16 × 0.09 × 0.08
λ / Å	0.71073
μ / mm^{-1}	5.373
Collection range	$1.536 \leq \theta \leq 30.592$ ° (h: −15 to 13; k: −37 to 37; l: −14 to 14)
Completeness to theta	0.992
No. of data collected	83311
No. of unique data	8435
No. of data used in refinement, m	7190
No. of parameters refined, p	345
R	0.0229
wR	0.0378
Goodness-of-fit, S	1.058
Maximum shift, $(\Delta/\sigma)_{max}$	0.003
Residual extrema in final difference map, eÅ^{-3}	+1.080, −0.717

Table S6. Selected bond distances (Å) and angles (°) with estimated standard deviations (esds) in parentheses for **1** and **2**.

		Selected bond lengths (Å)		
1	Pt(1)–N(1)	2.0828(14)	Pt(1)–C(19)	1.9566(16)
	Pt(1)–N(2)	2.0860(13)	C(11)–C(12)	1.212(2)
	Pt(1)–C(11)	1.9503(17)	C(19)–C(20)	1.210(2)
2	Pt(1)–N(1)	2.0839(16)	Pt(1)–C(19)	1.954(2)
	Pt(1)–N(2)	2.0858(16)	C(11)–C(12)	1.213(3)
	Pt(1)–C(11)	1.9559(19)	C(19)–C(20)	1.206(3)
	S(1)–O(1)	1.4893(15)		
		Selected bond angles (°)		
1	N(1)–Pt(1)–N(2)	88.35(5)	Pt(1)–C(11)–C(12)	176.01(15)
	C(11)–Pt(1)–C(19)	90.69(7)	Pt(1)–C(19)–C(20)	173.63(15)
	N(1)–Pt(1)–C(19)	176.92(6)	C(6)–S(1)–C(1)	100.00(8)
	N(2)–Pt(1)–C(11)	177.84(6)		
2	N(1)–Pt(1)–N(2)	88.88(6)	Pt(1)–C(11)–C(12)	175.45(18)
	C(11)–Pt(1)–C(19)	90.31(8)	Pt(1)–C(19)–C(20)	175.67(17)
	N(1)–Pt(1)–C(19)	177.61(7)	C(6)–S(1)–C(1)	96.06(9)
	N(2)–Pt(1)–C(11)	175.43(7)		

Table S7. Selected bond distances (Å) with estimated standard deviations (esds) in parentheses for **4**–**6**.

Selected bond lengths (Å)				
4	Pt(1)–N(1)	2.0899(13)	Pt(1)–C(21)	1.9509(16)
	Pt(1)–N(2)	2.0834(13)	C(13)–C(14)	1.188(2)
	Pt(1)–C(13)	1.9699(17)	C(21)–C(22)	1.203(2)
5	Pt(1)–N(1)	2.0873(19)	Pt(1)–C(21)	1.952(2)
	Pt(1)–N(2)	2.0843(18)	C(13)–C(14)	1.202(3)
	Pt(1)–C(13)	1.964(2)	C(21)–C(22)	1.201(3)
	S(1)–O(1)	1.4839(18)		
6	Pt(1)–N(1)	2.1048(18)	Pt(1)–C(21)	1.947(2)
	Pt(1)–N(2)	2.0844(18)	C(13)–C(14)	1.206(3)
	Pt(1)–C(13)	1.956(2)	C(21)–C(22)	1.204(3)
	S(1)–O(1)	1.4342(17)	S(1)–O(2)	1.4364(16)

Table S8. Selected bond angles (°) with estimated standard deviations (esds) in parentheses for **4**–**6**.

	Selected bond angles (°)			
4	N(1)–Pt(1)–N(2)	88.03(5)	Pt(1)–C(13)–C(14)	176.07(14)
	C(13)–Pt(1)–C(21)	88.42(6)	Pt(1)–C(21)–C(22)	177.73(14)
	N(1)–Pt(1)–C(21)	178.89(6)	C(7)–S(1)–C(1)	101.28(7)
	N(2)–Pt(1)–C(13)	177.73(5)		
5	N(1)–Pt(1)–N(2)	88.15(7)	Pt(1)–C(13)–C(14)	179.1(2)
	C(13)–Pt(1)–C(21)	89.37(9)	Pt(1)–C(21)–C(22)	178.0(2)
	N(1)–Pt(1)–C(21)	178.58(8)	C(7)–S(1)–C(1)	94.89(11)
	N(2)–Pt(1)–C(13)	178.23(8)		
6	N(1)–Pt(1)–N(2)	88.85(7)	Pt(1)–C(13)–C(14)	177.30(19)
	C(13)–Pt(1)–C(21)	91.81(9)	Pt(1)–C(21)–C(22)	170.3(2)
	N(1)–Pt(1)–C(21)	175.68(8)	C(7)–S(1)–C(1)	102.69(10)
	N(2)–Pt(1)–C(13)	179.33(8)	O(1)–S(1)–O(2)	119.05(10)

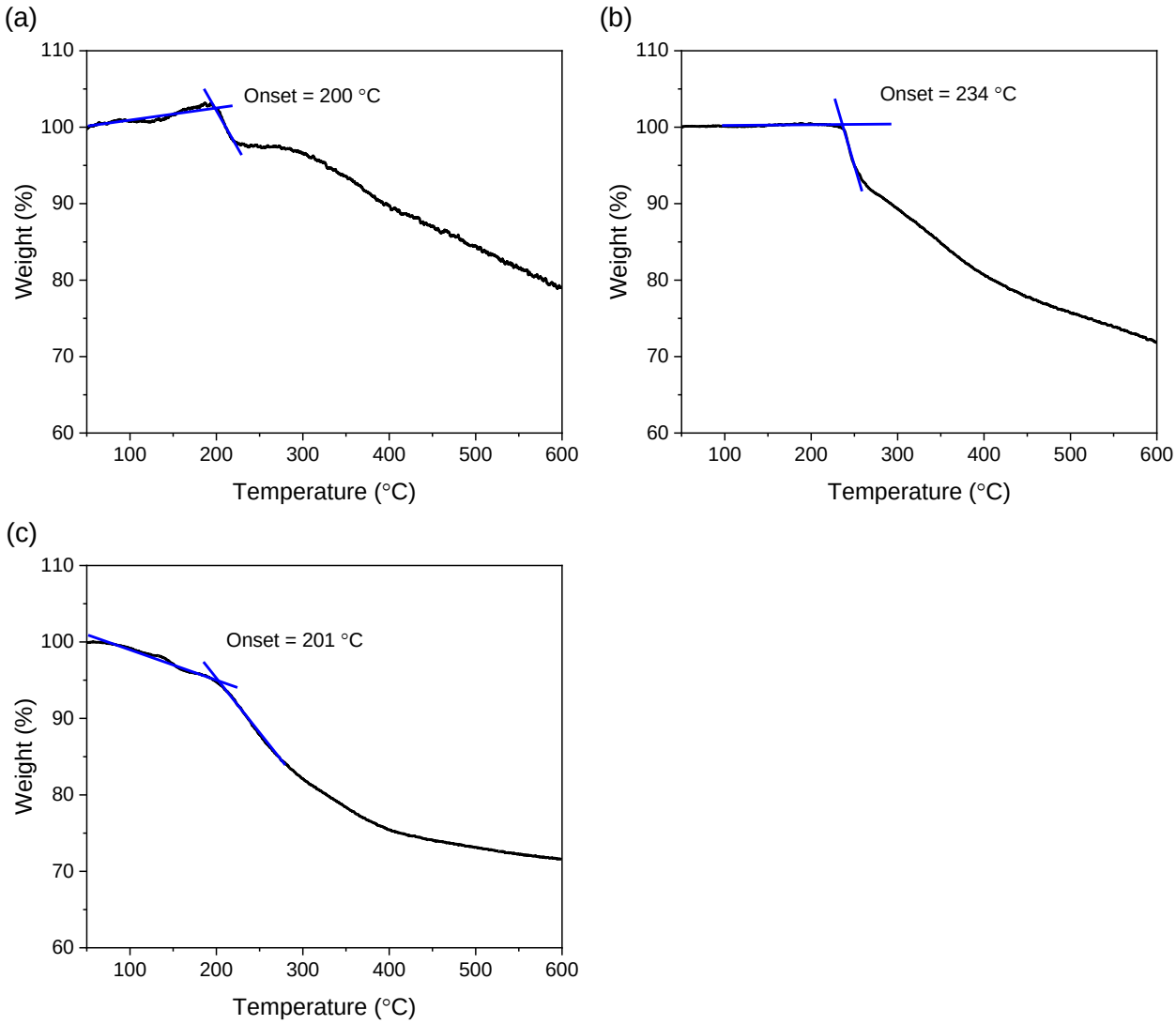

Figure S24. Thermogravimetric analysis of complexes (a) **1**, (b) **2** and (c) **3**.

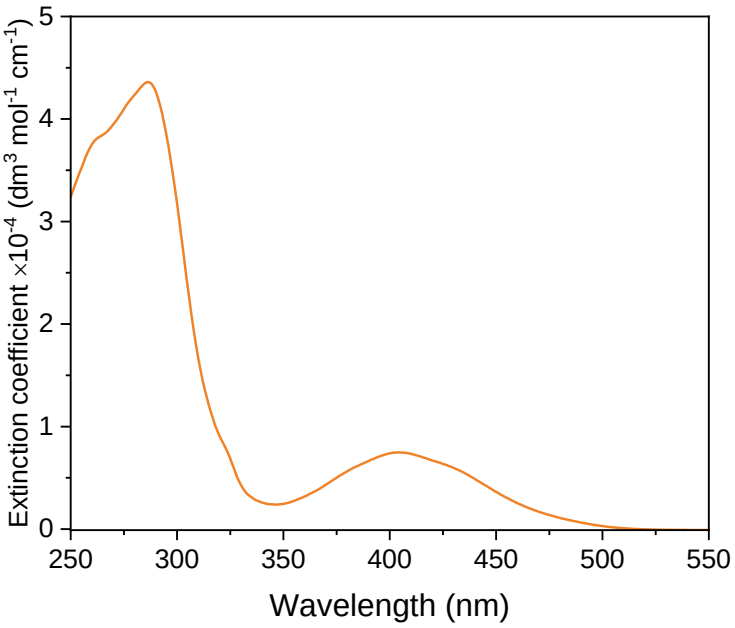

Figure S25. Electronic absorption spectra of **[Pt(bpy)(C≡CPh)$_2$]** in dichloromethane solution at 298 K.

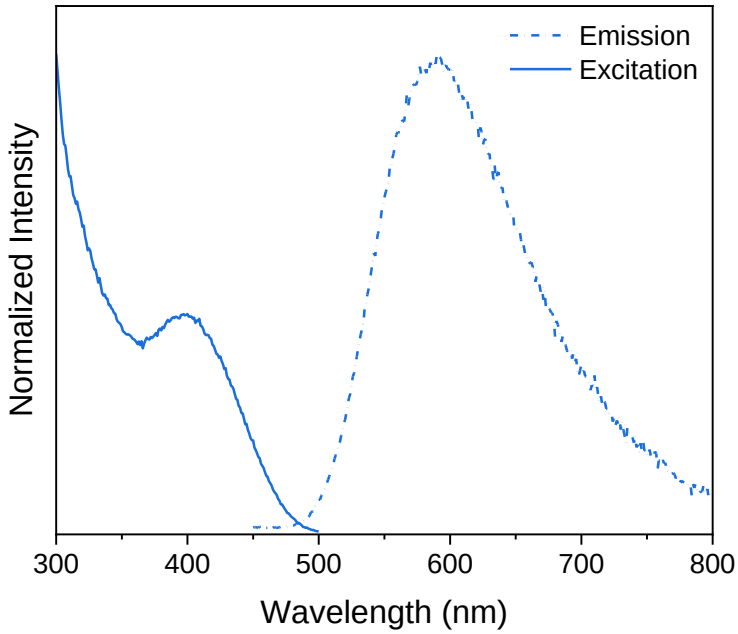

Figure S26. Normalized excitation (solid line) and emission (dot line) spectra of complexes **3** in dichloromethane solution at 298 K.

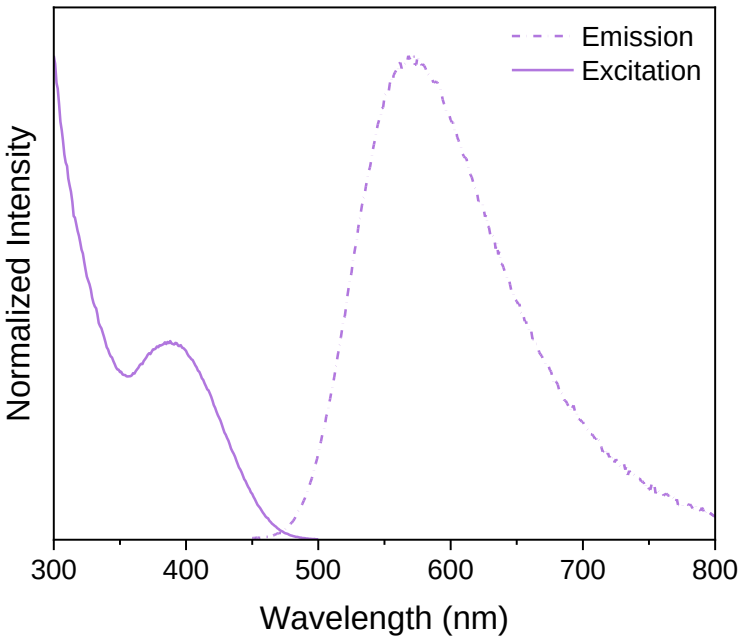

Figure S27. Normalized excitation (solid line) and emission (dot line) spectra of complexes **6** in dichloromethane solution at 298 K.

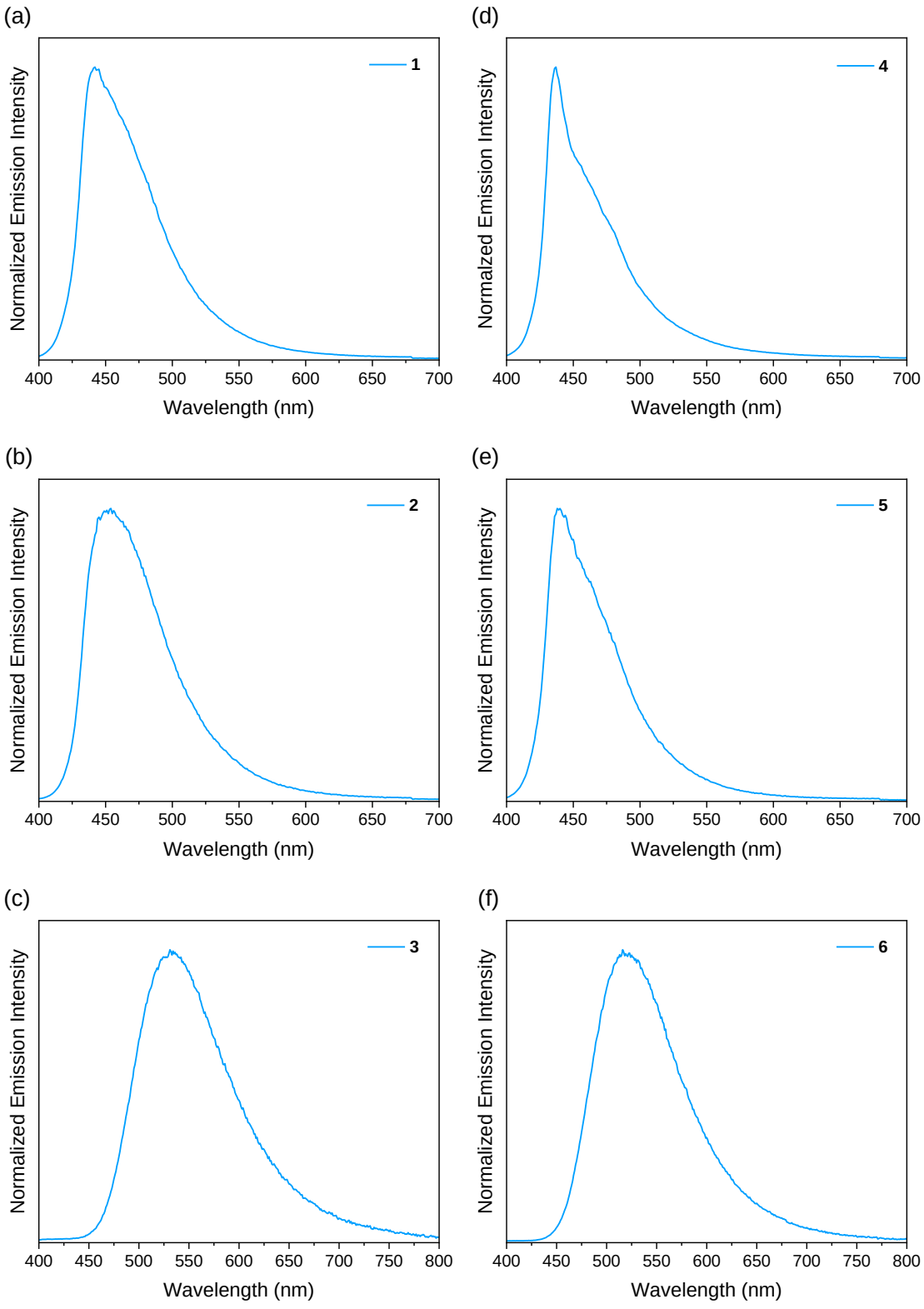

Figure S28. Photoluminescence spectra of the PMMA film (2 wt%) of (a) **1**, (b) **2**, (c) **3**, (d) **4**, (e) **5** and (f) **6** at 298 K.

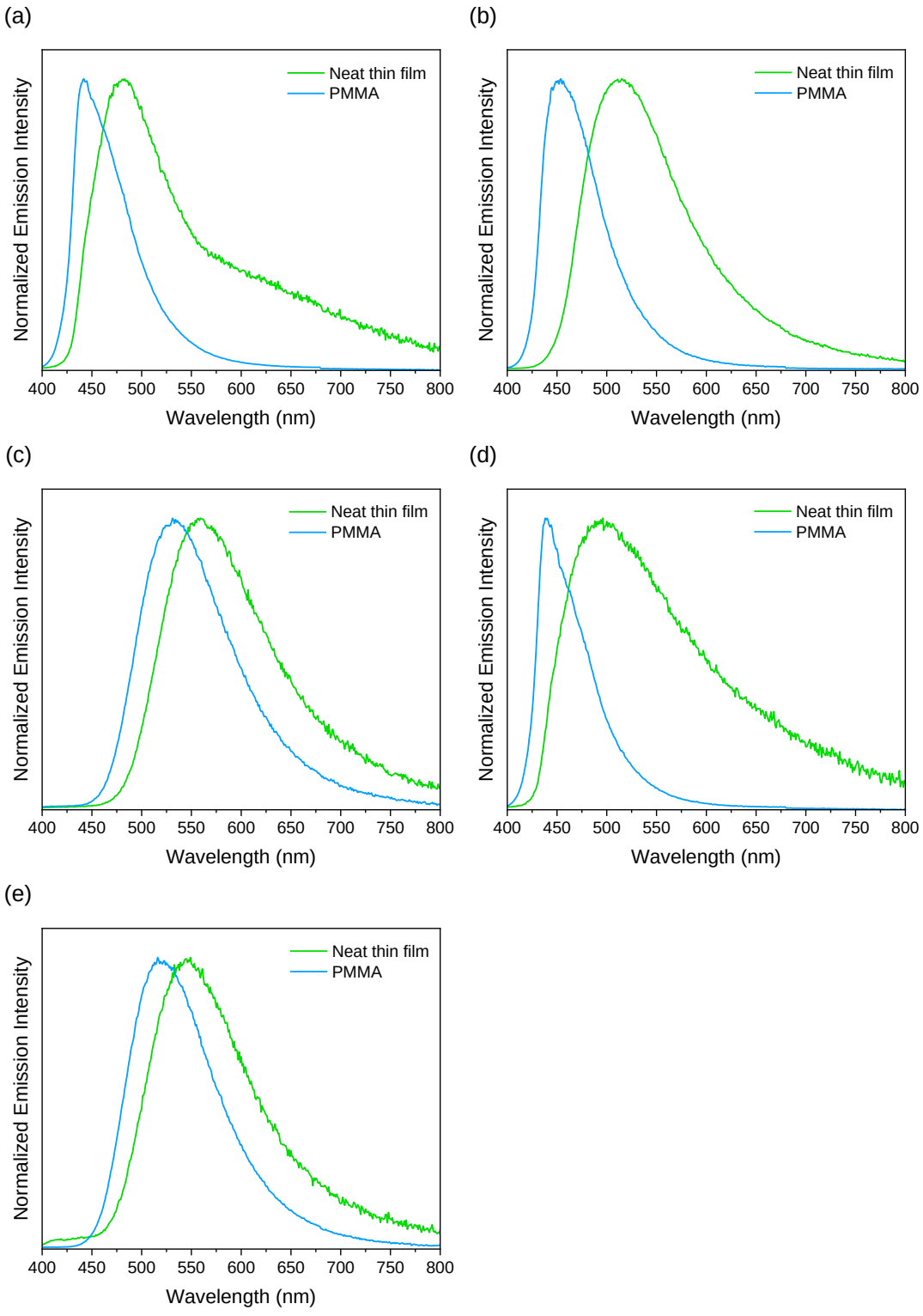

Figure S29. Overlaid photoluminescence spectra of the neat thin film and PMMA film (2 wt%) at 298 K of (a) **1**, (b) **2**, (c) **3**, (d) **5**, and (e) **6** (λ_{ex} = 365 nm).

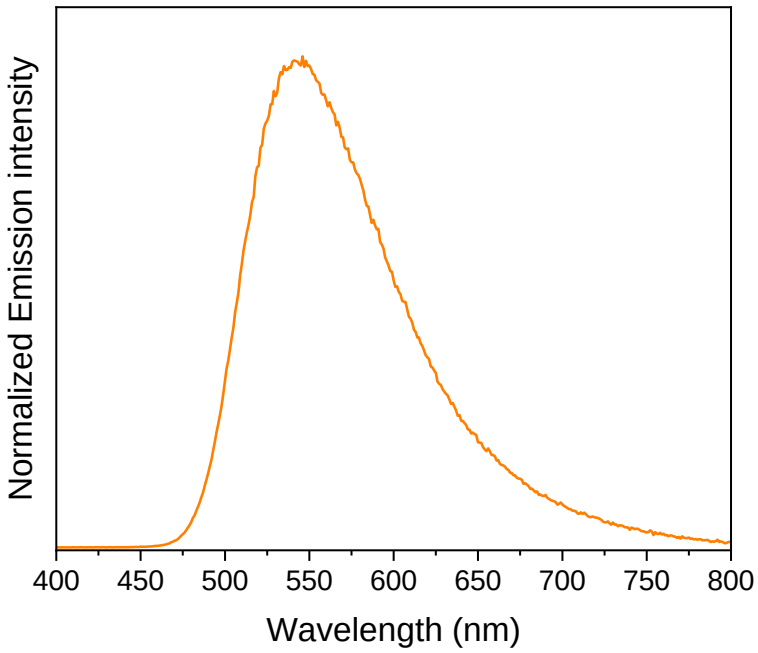

Figure S30. Photoluminescence spectra of a PMMA film (2 wt%) of **[Pt(bpy)(C≡CPh)$_2$]** at 298 K.

Table S9. CIE coordinates for complexes **1**–**6** and **[Pt(bpy)(C≡CPh)$_2$]**.

complex	CIE coordinates (CIE*x*, CIE*y*)	CIE*x* + CIE*y*
1	(0.15, 0.11)	0.26
2	(0.15, 0.14)	0.29
3	(0.34, 0.55)	0.89
4	(0.16, 0.10)	0.26
5	(0.15, 0.10)	0.25
6	(0.29, 0.53)	0.82
[Pt(bpy)(C≡CPh)$_2$]	(0.39, 0.57)	0.96

Table S10. Photophysical data for complexes **1**, **2**, **4**, **5** and other deep-blue Pt(II) complexes in 2% PMMA films reported in the literature.[15]

complex	Φ_{em}	complex	Φ_{em}
1	0.40	**Pt-4**	0.15
2	0.82	**Pt-5**	0.43
4	0.35	**Pt-6**	0.30
5	0.71	**Pt-7**	0.30
Pt-1	0.014	**Pt-8**	0.65
Pt-2	0.058	**Pt-9**	0.56
Pt-3	0.23	**Pt-10**	0.58
Pt-4	0.15		

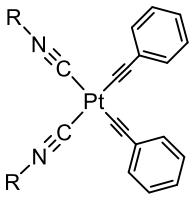

Pt-1: R = ^{t}Bu
Pt-2: R = 2,6-xylyl

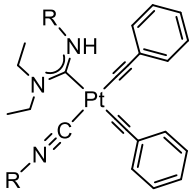

Pt-3: R = ^{t}Bu
Pt-4: R = 2,6-xylyl

Chem. Eur. J. **2020**

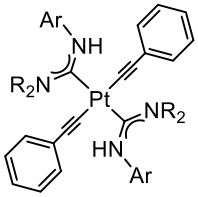

Pt-5: Ar = 2,6-xylyl ; R = C_2H_5
Pt-6: Ar = 2,6-xylyl ; R = CH_3

Chem. Sci. **2023**

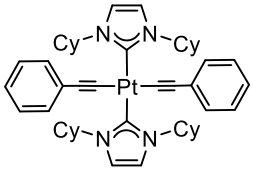

Pt-7

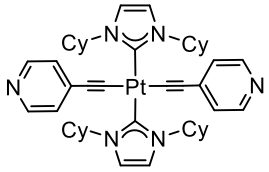

Pt-8

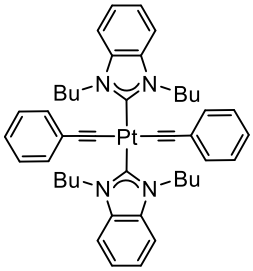

Pt-9

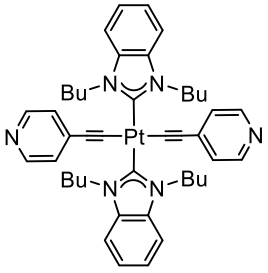

Pt-10

ACS Appl. Electron. Mater. **2020**

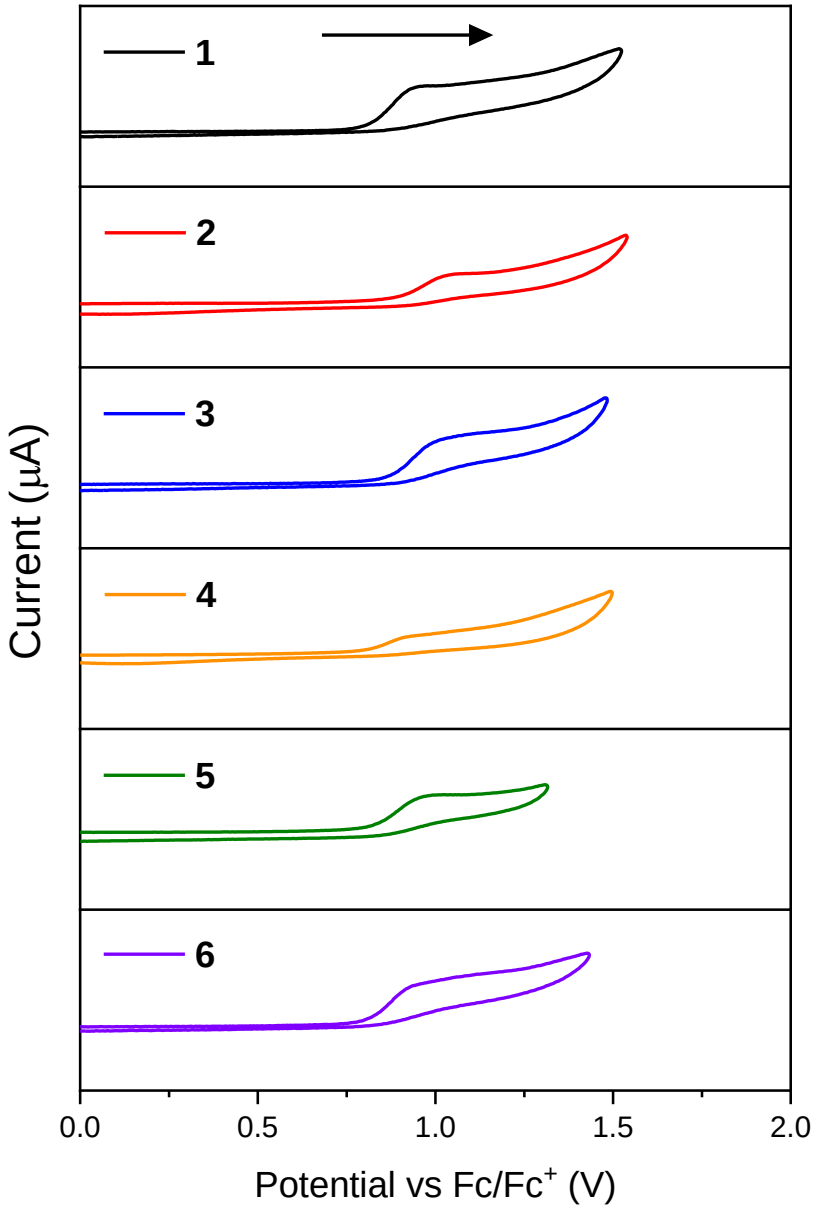

Figure S31. Oxidation waves of complexes **1**–**6** in acetonitrile solution (0.1 mol dm^{-3} $^{n}Bu_4NPF_6$) at a scan rate of 100 mVs^{-1} with Fc/Fc^+ employed as a reference.

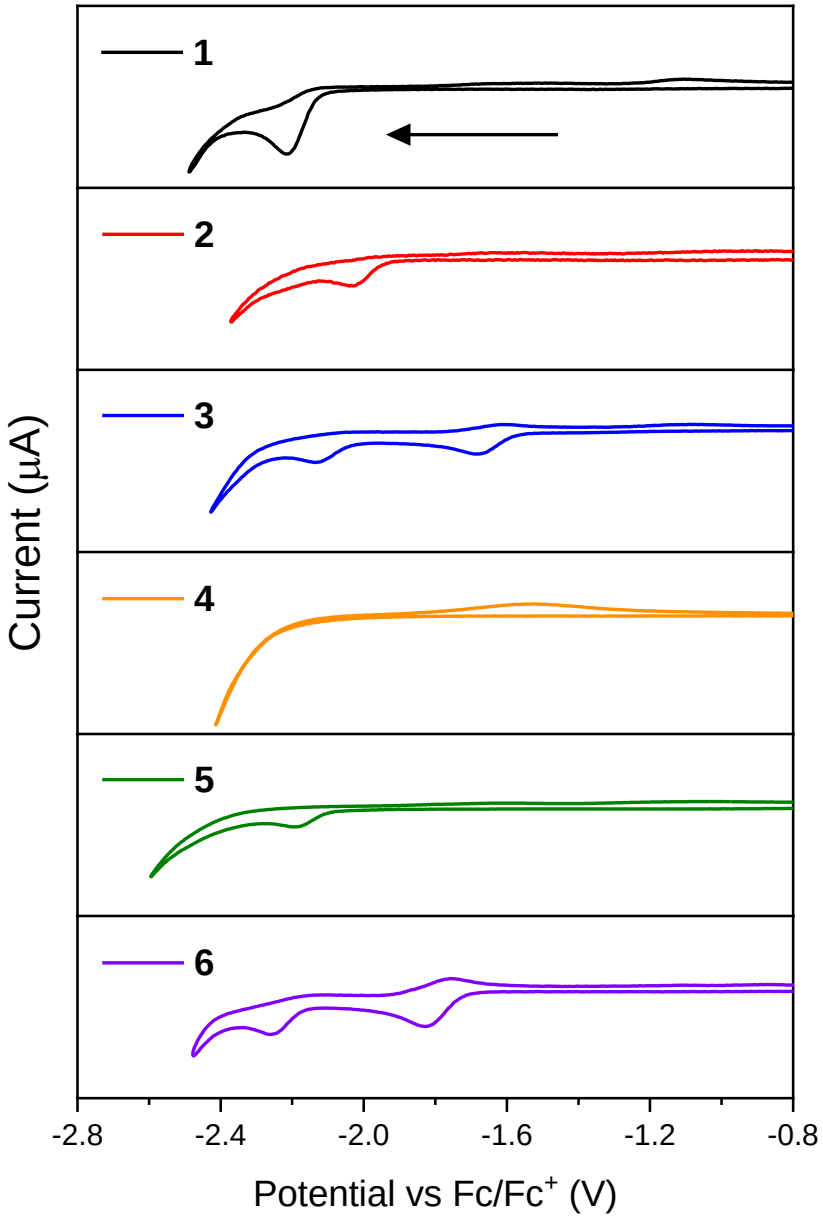

Figure S32. Reduction waves of complexes **1**–**6** in acetonitrile solution (0.1 mol dm^{-3} $^{n}Bu_4NPF_6$) at a scan rate of 100 mVs^{-1} with Fc/Fc^{+} employed as a reference.

Table S11. Selected bond lengths (Å), bond angles (°) at optimized S_0 and T_1 geometry of complexes **1–3** within PBE0/ZORA-def2-SVP and solvent correction (CPCM) level of theory and the root-mean-square deviation (RMSD) comparing the optimized T_1 and S_0 geometries.

complex	**1**		**2**		**3**	
	S_0	T_1	S_0	T_1	S_0	T_1
Pt(1)–N(1)	2.0921	2.08027	2.08772	2.07927	2.10025	2.0912
Pt(1)–N(2)	2.0907	2.08127	2.0883	2.07738	2.10076	2.09494
Pt(1)–C(11)	1.92696	1.89889	1.9278	1.89973	1.92754	1.8984
Pt(1)–C(19)	1.92718	1.8985	1.92919	1.8994	1.92636	1.90178
S(1)–O(1)	–	–	1.48096	1.48232	1.4297	1.43778
S(1)–O(2)	–	–	–	–	1.43792	1.44063
C(11)–C(12)	1.21584	1.23031	1.21534	1.23046	1.21523	1.22935
C(19)–C(20)	1.21582	1.23094	1.21545	1.23048	1.21531	1.22779
N(1)–Pt(1)–N(2)	90.44	87.966	89.633	87.451	91.184	88.476
C(11)–Pt(1)–C(19)	90.303	91.557	91.463	91.786	89.354	90.648
N(1)–Pt(1)–C(19)	179.07	177.235	177.241	177.413	177.668	177.136
N(2)–Pt(1)–C(11)	178.826	177.166	178.222	176.528	177.591	178.938
C(6)–S(1)–C(1)	102.742	96.893	95.427	91.961	103.272	99.168
O(1)–S(1)–O(2)	–	–	–	–	121.174	120.593
Pt(1)–C(11)–C(12)	175.665	177.085	175.34	176.903	176.963	178.493
Pt(1)–C(19)–C(20)	177.024	177.741	174.904	177.172	176.867	177.599
τ_4	0.015	0.040	0.032	0.043	0.034	0.028
RMSD	0.465		0.516		0.898	

Table S12. Selected bond lengths (Å), bond angles (°) at optimized S_0 and T_1 geometry of complexes **4**, **5** and **6** within PBE0/ZORA-def2-SVP and solvent correction (CPCM) level of theory and the root-mean-square deviation (RMSD) comparing the optimized T_1 and S_0 geometries.

complex	**4**		**5**		**6**	
	S_0	T_1	S_0	T_1	S_0	T_1
Pt(1)–N(1)	2.09193	2.08042	2.08722	2.07886	2.10161	2.09045
Pt(1)–N(2)	2.09133	2.08009	2.08867	2.07817	2.10039	2.09267
Pt(1)–C(13)	1.92724	1.89956	1.92823	1.89885	1.92772	1.89929
Pt(1)–C(21)	1.9263	1.89582	1.92915	1.90034	1.92629	1.90213
S(1)–O(1)	–	–	1.48169	1.48315	1.43009	1.43807
S(1)–O(2)	–	–	–	–	1.43858	1.44126
C(13) –C(14)	1.21603	1.23007	1.21549	1.23096	1.21544	1.22924
C(21)–C(22)	1.21594	1.23145	1.21556	1.23022	1.2154	1.22804
N(1)–Pt(1)–N(2)	90.45	88.244	89.381	87.231	91.058	88.587
C(13)–Pt(1)–C(21)	89.919	91.717	91.259	91.882	89.592	90.298
N(1)–Pt(1)–C(21)	178.702	176.5	177.359	176.059	178.133	177.453
N(2)–Pt(1)–C(13)	178.29	177.77	178.215	176.794	177.291	178.442
C(1)–S(1)–C(7)	102.825	96.778	95.239	91.337	103.322	99.244
O(1)–S(1)–O(2)	–	–	–	–	121.024	120.537
Pt(1)–C(13)–C(14)	176.067	176.358	175.903	177.182	176.736	178.71
Pt(1)–C(21)–C(22)	176.912	177.834	175.601	176.038	176.645	178.226
τ_4	0.021	0.041	0.031	0.051	0.032	0.029
RMSD	0.496		0.596		0.954	

Figure S33. Ground-state frontier orbitals for the complexes **1**–**3**.

Complex 1

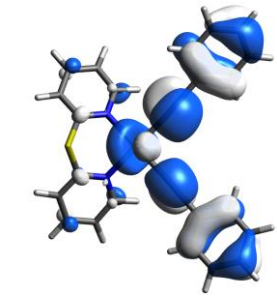

HOMO–1

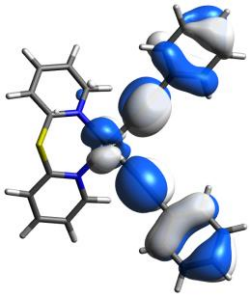

HOMO

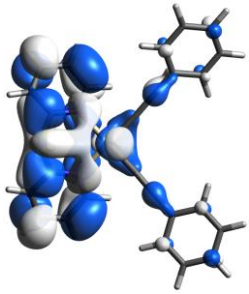

LUMO

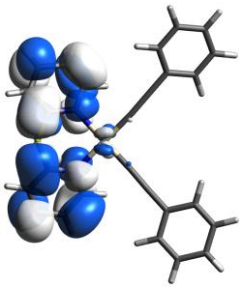

LUMO+1

Complex 2

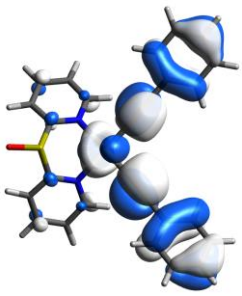

HOMO–1

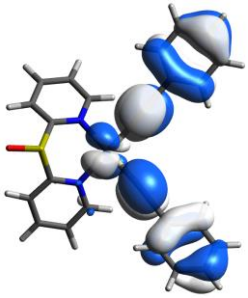

HOMO

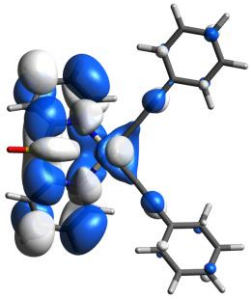

LUMO

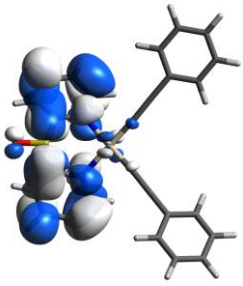

LUMO+1

Complex 3

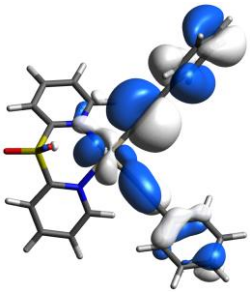

HOMO–1

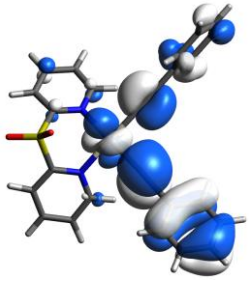

HOMO

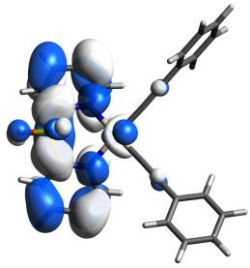

LUMO

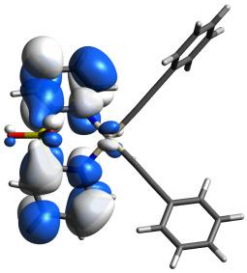

LUMO+1

Figure S34. Ground-state frontier orbitals for the complexes **4**–**6.**

Complex 4

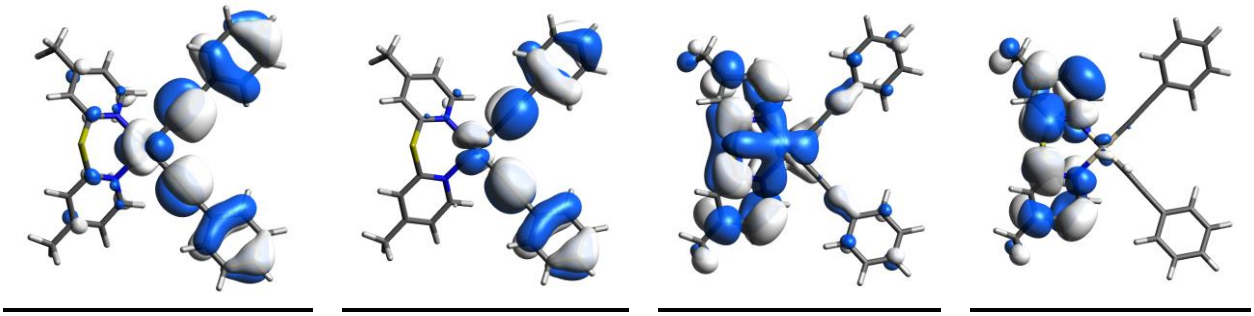

HOMO–1 | HOMO | LUMO | LUMO+1

Complex 5

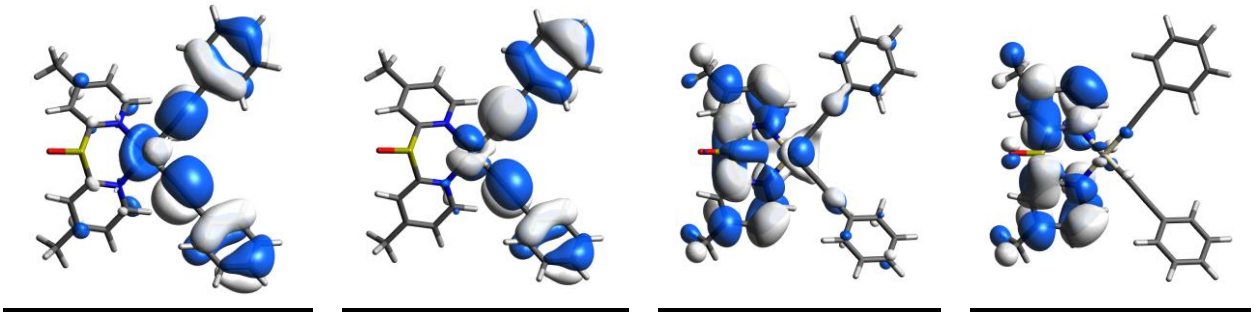

HOMO–1 | HOMO | LUMO | LUMO+1

Complex 6

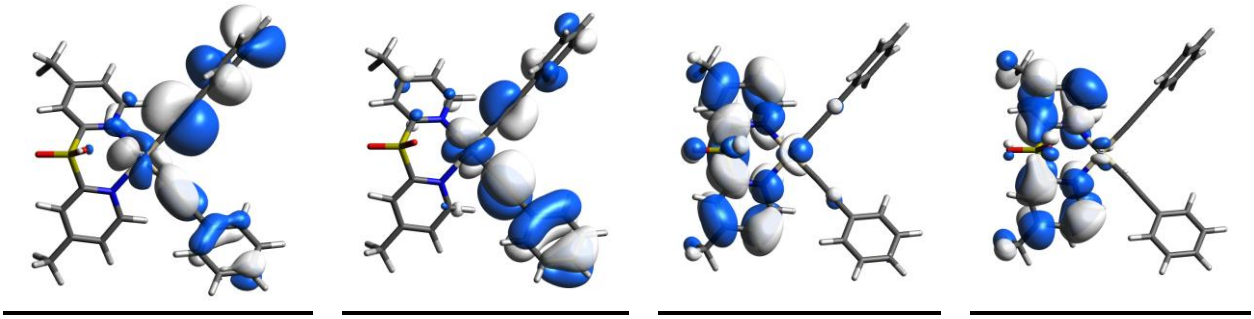

HOMO–1 | HOMO | LUMO | LUMO+1

Table S13. Ground-state frontier orbital energies for the complexes **1**–**6** within PBE0/def2-TZVP(-f) and ZORA scalar-relativistic corrections level of theory.

	orbitals energy (eV)			
complex	HOMO–1	HOMO	LUMO	LUMO+1
1	–6.08	–5.93	–1.93	–1.81
2	–6.14	–6.03	–2.15	–1.82
3	–6.20	–6.07	–2.58	–1.91
4	–6.02	–5.91	–1.78	–1.65
5	–6.11	–5.98	–1.98	–1.64
6	–6.17	–6.03	–2.41	–1.73

Table S14. Selected excited states of complexes **1**–**3** with vertical excitation and oscillator strength calculated by TD-DFT at optimized geometries within PBE0/def2-SVP(-f) and ZORA scalar-relativistic corrections level of theory.

complex	state[a]	excitation (contribution)[b]	nature of transition	energy (eV)	oscillator strength (*f*)
1	S_1	H → L (0.92)	MLCT, LLCT	3.26	0.1421
	S_2	H → L+1 (0.55)	MLCT, LLCT	3.35	0.0390
		H-1 → L (0.43)	MLCT, LLCT		
	S_3	H–1 → L (0.52)	MLCT, LLCT	3.51	0.3187
		H → L+1 (0.42)	MLCT, LLCT		
	S_4	H-1 → L+1 (0.88)	MLCT, LLCT	3.54	0.1103
	S_{14}	H → L+4 (0.91)	MLCT, LLCT, *d*-*d*	4.36	0.4629
2	S_1	H → L (0.96)	MLCT, LLCT	3.16	0.1374
	S_2	H–1 → L (0.88)	MLCT, LLCT	3.27	0.1714
	S_3	H → L+1 (0.86)	MLCT, LLCT	3.53	0.0994
	S_4	H–1 → L+1 (0.93)	MLCT, LLCT	3.61	0.0907
	S_{13}	H → L+4 (0.87)	MLCT, LLCT, *d*-*d*	4.36	0.4299
3	S_1	H → L (0.97)	MLCT, LLCT	2.78	0.0993
	S_3	H–2 → L (0.94)	MLCT, LLCT	3.25	0.0970
	S_8	H → L+2 (0.92)	MLCT, LLCT	3.80	0.1059
	S_{10}	H–1 → L+2 (0.66)	MLCT, LLCT	3.94	0.0948
		H–2 → L+1 (0.26)	MLCT, LLCT		
	S_{19}	H → L+4 (0.73)	MLCT, LLCT, *d*-*d*	4.55	0.4896

[a] Vertical states taking S_0 geometry as the reference; [b] Transitions high percentage higher than 20% are shown in parenthesis.

Table S15. Selected excited states of complexes **4–6** with vertical excitation and oscillator strength calculated by TD-DFT at optimized geometries within PBE0/def2-SVP(-f) and ZORA scalar-relativistic corrections level of theory.

complex	state[a]	excitation (contribution)[b]	nature of transition	energy (eV)	oscillator strength (*f*)
4	S_1	H → L (0.91)	MLCT, LLCT	3.39	0.1627
	S_2	H–1 → L (0.62)	MLCT, LLCT	3.47	0.1121
		H → L+1 (0.35)	MLCT, LLCT		
	S_3	H → L+1 (0.58)	MLCT, LLCT	3.62	0.2771
		H–1 → L (0.33)	MLCT, LLCT		
	S_4	H–1 → L+1 (0.86)	MLCT, LLCT	3.65	0.1487
	S_{14}	H → L+4 (0.89)	MLCT, LLCT, *d*-*d*	4.38	0.4210
5	S_1	H → L (0.96)	MLCT, LLCT	3.28	0.1517
	S_2	H–1 → L (0.89)	MLCT, LLCT	3.41	0.2082
	S_3	H → L+1 (0.87)	MLCT, LLCT	3.66	0.1042
	S_4	H–1 → L+1 (0.53)	MLCT, LLCT	3.76	0.0589
		H–2 → L (0.40)	MLCT, LLCT		
	S_5	H–2 → L (0.52)	MLCT, LLCT	3.77	0.0943
		H–1 → L+1 (0.41)	MLCT, LLCT		
	S_{13}	H → L+4 (0.92)	MLCT, LLCT, *d*-*d*	4.34	0.4630
6	S_1	H → L (0.97)	MLCT, LLCT	2.92	0.1056
	S_3	H–2 → L (0.95)	MLCT, LLCT	3.36	0.1047
	S_8	H → L+2 (0.78)	MLCT, LLCT	3.83	0.1469
	S_{10}	H–2 → L+2 (0.88)	MLCT, LLCT	4.04	0.0920
	S_{19}	H → L+4 (0.63)	MLCT, LLCT, *d*-*d*	4.54	0.4107

[a] Vertical states taking S_0 geometry as the reference; [b] Transitions high percentage higher than 20% are shown in parenthesis.

Table S16. Selected excited states of **1**–**6** with vertical excitation and oscillator strength calculated by SOC-TD-DFT at optimized geometries within PBE0/def2-SVP(-f) and ZORA scalar-relativistic corrections level of theory.

complex	state[a]	excitation (contribution)[b]	nature of transition	energy (eV)	oscillator strength (*f*)[c]
1	T_1	H → L (0.73)	MLCT, LLCT	3.02	1.60×10^{-3}
	T_2	H–1 → L (0.69)	MLCT, LLCT	3.11	5.46×10^{-3}
2	T_1	H → L (0.80)	MLCT, LLCT	2.98	2.70×10^{-3}
	T_2	H–1 → L (0.80)	MLCT, LLCT	3.04	7.98×10^{-3}
3	T_1	H → L (0.94)	MLCT, LLCT	2.67	8.46×10^{-3}
4	T_1	H → L (0.63)	MLCT, LLCT	3.09	1.53×10^{-3}
	T_2	H–1 → L (0.61)	MLCT, LLCT	3.16	2.86×10^{-3}
5	T_1	H → L (0.69)	MLCT, LLCT	3.04	2.12×10^{-3}
	T_2	H–1 → L (0.68)	MLCT, LLCT	3.14	7.23×10^{-3}
6	T_1	H → L (0.91)	MLCT, LLCT	2.79	8.50×10^{-4}

[a] Vertical states taking S_0 geometry as the reference; [b] Transitions high percentage higher than 20% are shown in parenthesis; [c] *f* for the triplet states is shown as an average of the substates x, y and z.

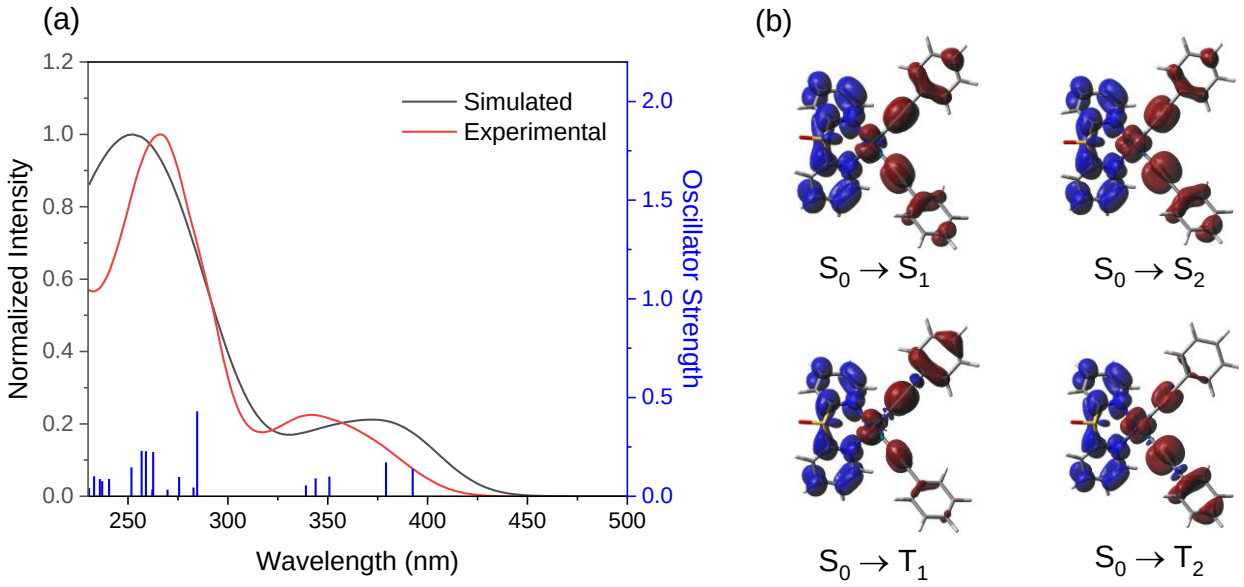

Figure S35. (a) Simulated (black trace) and experimental (red trace) electronic absorption spectra for complex **2**. Transition energies and oscillator strengths calculated from TD-DFT calculations are shown by blue vertical lines, and the simulated spectrum is deconvoluted with Gaussian functions. (b) Electronic difference plots with the accumulation (blue) and depletion (red) of charge for the lowest-energy transitions and the triplet states.

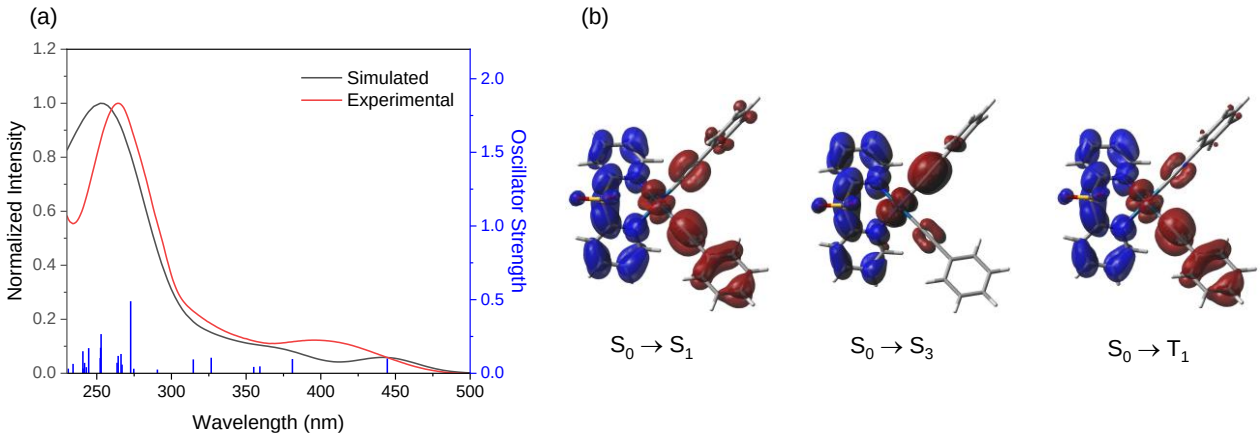

Figure S36. (a) Simulated (black trace) and experimental (red trace) electronic absorption spectra for complex **3**. Transition energies and oscillator strengths calculated from TD-DFT calculations are shown by blue vertical lines, and the simulated spectrum is deconvoluted with Gaussian functions. (b) Electronic difference plots with the accumulation (blue) and depletion (red) of charge for the lowest-energy transitions and the triplet states.

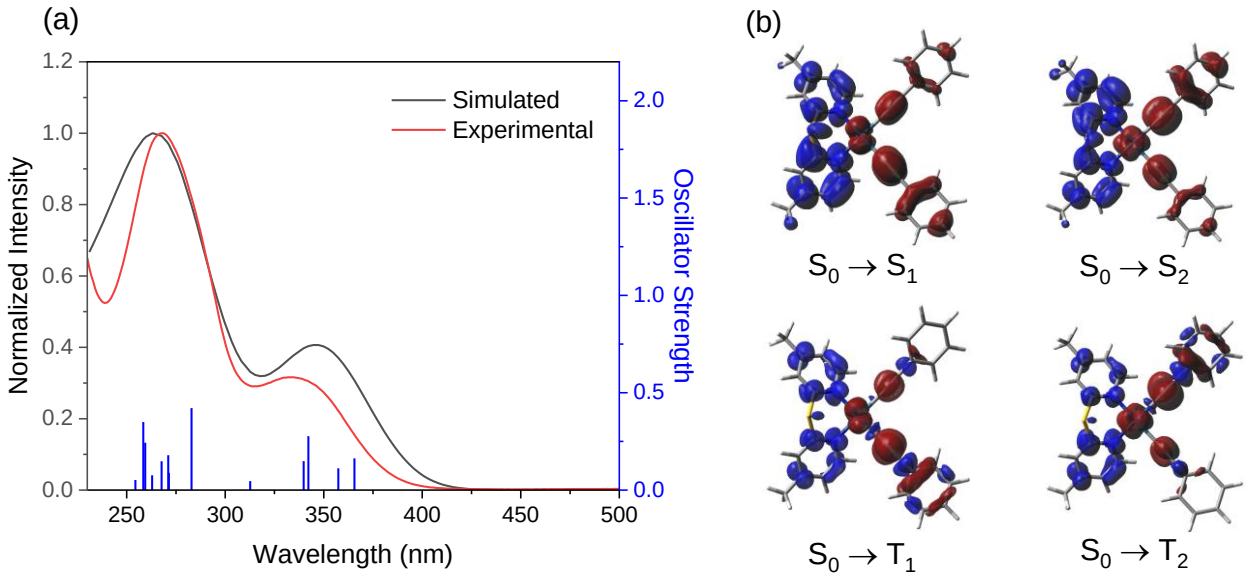

Figure S37. (a) Simulated (black trace) and experimental (red trace) electronic absorption spectra for complex **4**. Transition energies and oscillator strengths calculated from TD-DFT calculations are shown by blue vertical lines, and the simulated spectrum is deconvoluted with Gaussian functions. (b) Electronic difference plots with the accumulation (blue) and depletion (red) of charge for the lowest-energy transitions and the triplet states.

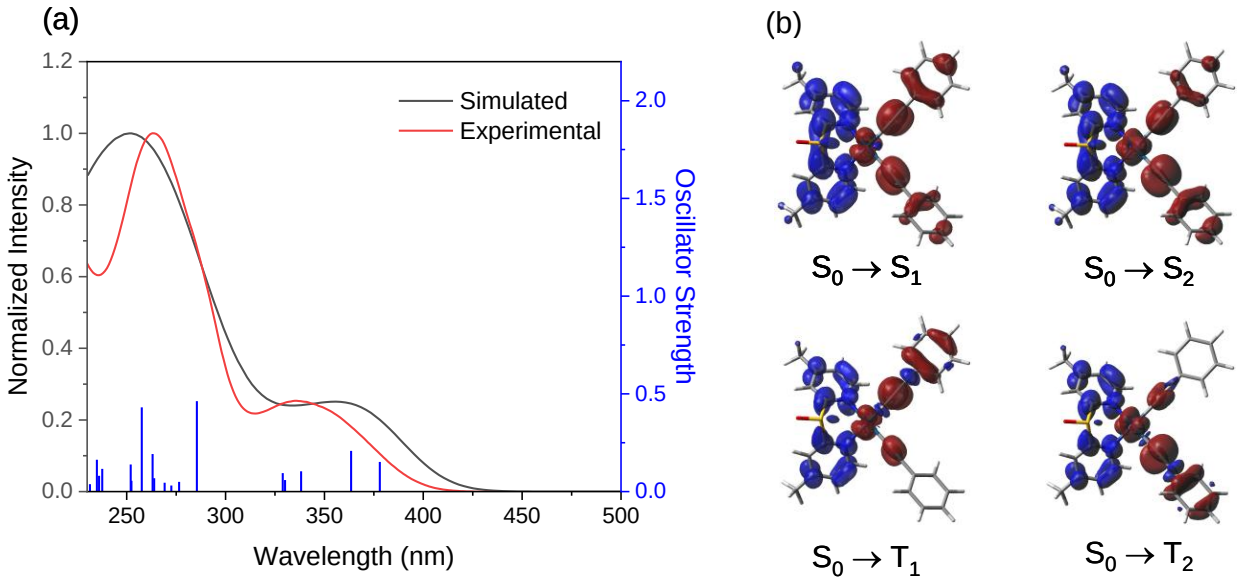

Figure S38. (a) Simulated (black trace) and experimental (red trace) electronic absorption spectra for complex **5**. Transition energies and oscillator strengths calculated from TD-DFT calculations are shown by blue vertical lines, and the simulated spectrum is deconvoluted with Gaussian functions. (b) Electronic difference plots with the accumulation (blue) and depletion (red) of charge for the lowest-energy transitions and the triplet states.

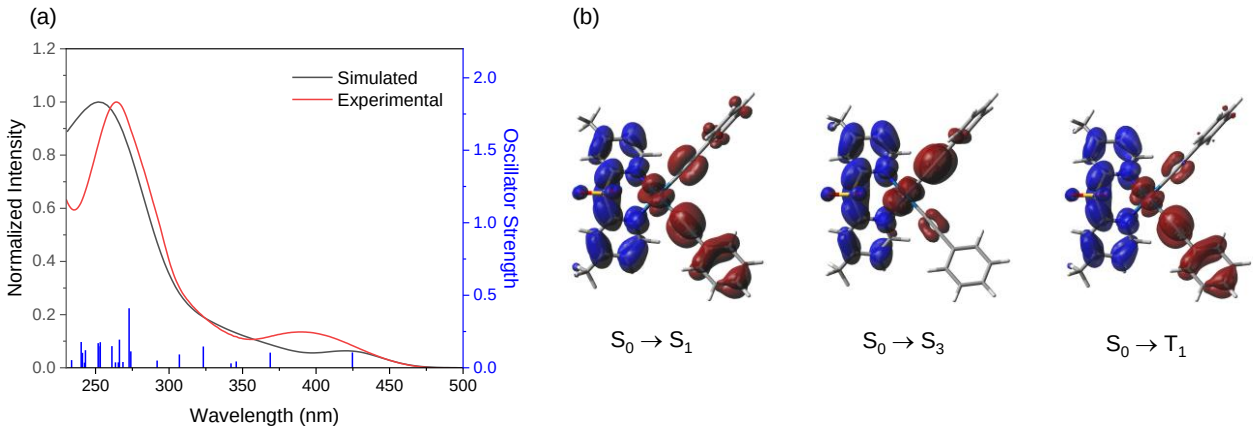

Figure S39. (a) Simulated (black trace) and experimental (red trace) electronic absorption spectra for complex **6**. Transition energies and oscillator strengths calculated from TD-DFT calculations are shown by blue vertical lines, and the simulated spectrum is deconvoluted with Gaussian functions. (b) Electronic difference plots with the accumulation (blue) and depletion (red) of charge for the lowest-energy transitions and the triplet states.

Table S17. Data of SOCME (in cm^{-1}) at optimized S_0 geometry within PBE0/def2-SVP(-f) and ZORA scalar-relativistic corrections level of theory for complexes **1**–**6**.

complex	**1**	**2**	**3**	**4**	**5**	**6**
$\langle T_1\|H_{SO}\|S_0\rangle$[a]	102	165	237	54	127	209
$\langle T_2\|H_{SO}\|S_0\rangle$[a]	123	57	[b]	86	59	[b]
$\sum\langle T_n\|H_{SO}\|S_0\rangle$	225	223	237	140	187	209
$\langle T_1\|H_{SO}\|S_1\rangle$[a]	77	126	117	50	141	119
$\langle T_2\|H_{SO}\|S_1\rangle$[a]	562	588	[b]	534	556	[b]
$\sum\langle T_n\|H_{SO}\|S_1\rangle$	639	714	117	584	697	119

[a] $\sqrt{\langle(S_i|H_{SO}|T_j)^2\rangle}$ in the S_0 geometry. [b] T_2 state is not considered because it has a higher energy than S_1.

Table S18. Calculated adiabatic, vertical transition within PBE0/def2-SVP(-f) and ZORA scalar-relativistic corrections level of theory and experimental emission in solid energies for complexes **1**–**6**.

complex	adiabatic energy ΔE (eV)	SOC T_1 (S_0) (eV)	experimental E_{em} (eV)
1	2.46	3.02	2.81
2	2.40	2.98	2.74
3	1.98	2.67	2.33
4	2.53	3.09	2.84
5	2.48	3.04	2.82
6	2.04	2.79	2.39

References

1. H. Lang, P. Zoufalá, S. Klaib, A. del Villar, G. Rheinwald, *J. Organomet. Chem.* 2007, **692**, 4168–4176.

2. C. M. Brown, M. Kitt, Z. Xu, D. Hean, M Ezhova, M. O. Wolf, *Inorg. Chem.* 2017, **56**, 15110−15118.

3. J. N. Demas, G. A. Crosby, *J. Phys. Chem.* 1971, **75**, 991–1024.

4. SAINT, Version 8.40B; Bruker AXS Inc.: Madison, WI, USA, 2019.

5. L. Krause, R. Herbst-Irmer, G. M. Sheldrick, D. Stalke, *J. Appl. Crystallogr.* 2015, **48**, 3–10.

6. O. V. Dolomanov, L. J. Bourhis, R. J. Gildea, J. A. K. Howard, H. Puschmann, *J. Appl. Crystallogr.* 2009, **42**, 339–341.

7. G. M. Sheldrick, *Acta Cryst.* 2015, **C71**, 3–8.

8. F. Neese, *WIREs Comput. Mol. Sci.* 2022, **12**, e1606.

9. (a) J. P. Perdew, K. Burke, M. Ernzerhof, *Phys. Rev. Lett.* 1996, **77**, 3865–3868. (b) J. P. Perdew, K. Burke, M. Ernzerhof, *Phys. Rev. Lett.* 1997, **78**, 1396–1396.

10. (a) F. Weigend, R. Ahlrichs, *Phys. Chem. Chem. Phys.* 2005, **7**, 3297–3305. (b) A. Schäfer, C. Huber, R. Ahlrichs, *J. Chem. Phys.* 1994, **100**, 5829–5835. (c) D. A. Pantazis, X.-Y. Chen, C. R. Landis, F. Neese, *J. Chem. Theory Comput*. 2008, **4**, 908–919.

11. (a) S. Grimme, J. Antony, S. Ehrlich, H. Krieg, *J. Chem. Phys.* 2010, **132**, 154104. (b) S. Grimme, S. Ehrlich, L. Goerigk, *J. Comput. Chem.* 2011, **32**, 1456–1465.

12. T. Petrenko, S. Kossmann, F. Neese, *J. Chem. Phys.* 2011, **134**, 054116.

13. J. Tomasi, B. Mennucci, R. Cammi, *Chem. Rev.* 2005, **105**, 2999–3094.

14. (a) B. de Souza, F. Neese, R. Izsák, *J. Chem. Phys.* 2018, **148**, 034104. (b) B. de Souza, G. Farias, F. Neese, R. Izsák, *J. Chem. Theory Comput.* 2019, **15**, 1896–1904.

15. (a) Y. Wu, Z. Wen, J. I.-C. Wu, T. S. Teets, *Chem. Eur. J.* 2020, **26**, 16028–16035. (b) J. D. Bullock, Z. Xu, S. Valandro, M. Younus, J. Xue, K. S. Schanze, *ACS Appl. Electron. Mater.* 2020, **2**, 1026−1034. (c) Y. H. Nguyen, V. Q. Dang, J. V. Soares, J. I. Wu, T. S. Teets, *Chem. Sci.*, 2023, **14**, 4857–4862.